Drivers of seasonal hydrography in Disko Bay, Greenland

Linda Latuta[1,2], Lars H. Smedsrud[1,2], Elin Darelius[1,2], Per Juel Hansen[3], and Josh K. Willis[4]

[1]Geophysical Institute, University of Bergen, Bergen, Norway
[2]Bjerknes Centre for Climate Research, Bergen, Norway
[3]Department of Biology, Marine Biological Station, University of Copenhagen, Helsingør, Denmark
[4]Jet Propulsion Laboratory, California Institute of Technology, Pasadena, CA, USA

Correspondence: Linda Latuta (linda.latuta@uib.no)

Abstract.

This study investigates the seasonal dynamics of Disko Bay ~~in West~~ (Qeqertarsuup Tunua) in west Greenland. On the eastern side, the ~~hydrography in the bayis driven~~ bay's hydrography is influenced by ice-ocean interactions and exchange with Ilulissat Icefjord ~~, and~~ (Kangiata Sullua), while on the western side, ~~it~~ the bay exchanges waters with Baffin Bay. Since the mid-1990s, this region has experienced ~~significant changes, including rapid~~ ocean warming, sea-ice decline, and the retreat of Greenland's fastest-flowing marine-terminating glacier. Although West Greenland Irminger Water (WGIW) is known to be a significant heat source behind ~~many of~~ these changes, ~~it has remained unclear when and how these dense warm waters flow~~ the timing and pathways of its entry into Disko Bay remain poorly understood. We present a ~~2-year hydrographic record of observations within Disko Bay , determining the key hydrographic seasonality and the processes that drive it. Dense water renewal occurs repeatedly each springwhen~~ two-year (2022–2024) observational record of Disko Bay hydrography, providing new insights into the seasonal evolution and spatial structure of Polar Water (PW) and WGIW. Each spring, dense WGIW crosses the ~~sill~~ topographic barrier between Baffin Bay and Disko Bay~~. This spring renewal leads to the~~ , filling the Disko Bay basin and producing the highest observed temperature and ~~densest waters at depth, which rise high enough in the water column to reach~~ density at depth. The PW–WGIW boundary shoals to depths shallow enough for WGIW to renew the Ilulissat Icefjord ~~sill. Additionally, we show that renewal may occur in late autumnand winter in the presence of~~ basin. In autumn/winter 2022, an additional episodic renewal coincided with strong upwelling-favourable winds along the ~~West~~ west Greenland shelf. ~~Following the renewal-driven season in spring , the~~ While WGIW renewal dominates winter and spring seasonality (a period also marked by sea-ice presence), summer and autumn ~~are characterised by a deep-reaching fresh signal that extends over the upper 150 m across large areas of Disko Bay. Spatial analysis reveals an advective path that transports this fresh signal westward from the vicinity of Ilulissat Icefjord, along the northern periphery of the bay. Additional seasonal influence comes from along-isopycnal warming below this fresh layer, which is observed throughout autumn.~~ hydrography are shaped by PW. With the onset of the melt season, a fresh stratified layer forms in the upper 50 m and progressively thickens and extends downward, continuing to freshen and cool through autumn. Beneath this layer, denser PW warms steadily along isopycnals, with spatial analyses indicating an advective pathway transporting this warming signal along the bay's periphery.

1 Introduction

Disko Bay (Qeqertarsuup Tunua) is the largest open-water embayment in ~~West~~ west Greenland (Fig. 1). Bordered by Baffin Bay to the west and numerous glacial fjords to the east, its hydrography is shaped by a complex interplay of regional water mass exchanges, local oceanographic processes, and ice-ocean interactions. Since the late 1960s, oceanographic studies ~~in Disko Bay~~ have provided valuable insights into its hydrography and circulation patterns (Petersen, 1964; Muench, 1971; Andersen, 1981a). Subsequent research explored seasonality and ~~the associated~~ ecosystem functioning (Andersen, 1981b; Nielsen TG and Hansen B, 1995), while more recent studies have documented significant changes in ~~the~~ oceanographic conditions over the ~~past~~ recent decades (Hansen et al., 2012; Myers and Ribergaard, 2013). ~~A notable transition occurred~~

One of the most notable changes was a transition in the mid-1990s, when the increased presence of warm Atlantic-origin waters marked the ~~transition~~ shift from a cold to a warm regime in Disko Bay (Holland et al., 2008; Hansen et al., 2012). This warming was particularly evident at 200-250 m depth, ~~corresponding to the depth at which warm waters can enter Ilulissat Icefjord. By the late 1990s, temperatures at this depth had risen~~ where temperatures rose from ~1.5°C in the early 1990s to ~2-2.5°C by the late 1990s, eventually surpassing 3°C in the early 2000s (Hansen et al., 2012; Khazendar et al., 2019; Joughin et al., 2020). ~~This warming has been linked~~

These warm waters, upon entering Ilulissat Icefjord (Kangiata Sullua) above its 245 m sill (Fig.1b), have contributed to the disintegration of the floating ice tongue~~and the~~ , retreat, acceleration, and increased melting of Sermeq Kujalleq (Jakobshavn Glacier), Greenland's fastest flowing marine-terminating glacier ~~, located within Ilulissat Icefjord (Holland et al., 2008; Motyka et al., 2011 . Sermeq Kujalleq's response~~ (Joughin et al., 2004; Holland et al., 2008; Motyka et al., 2011; Khazendar et al., 2019; Joughin et al., 2020; . More recently, oceanic forcing has also been linked to a period of slowdown, thickening, and terminus re-advance in 2016-2018 (Joughin et al., 2018, 2020), as well as to renewed acceleration and increased solid ice discharge in subsequent years (Picton et al., 2025). Because Sermeq Kujalleq is highly sensitive to oceanic forcing~~and the exchange of water masses between Disko Bay and Ilulissat Icefjord (Gladish et al., 2015a) highlights the importance of continued monitoring to better understand the oceanographic processes governing these interactions~~, and the waters that fill Ilulissat Icefjord originate in Disko Bay (Gladish et al., 2015a), an improved understanding and continued monitoring of Disko Bay's hydrography is essential.

~~Despite extensive~~ Although Disko Bay has been the focus of long-term observations, ~~most available data were collected from Aprilto September, leaving gaps in our understanding of seasonal oceanographic variability. Winter sea-ice cover and harsh conditions have historically limited data collection, making it difficult to obtain sufficient temporal and spatial data coverage to determine~~ data coverage is biased toward April—September period. As a result, key processes such as the seasonality of ~~water masses in Disko Bay. In particular, the seasonality of~~ warm subsurface waters ~~remains~~ remain poorly understood. While it has been hypothesised that these deep warm waters renew in Disko Bay ~~renew during winter /~~during winter and early spring (Gladish et al., 2015a), the lack of ~~winter and early spring observations~~ observations during these seasons has left this process largely unexplored. ~~Moreover, Disko Bay is a recipient of glacially modified waters exported from Ilulissat Icefjord. While detailed studies have examined these waters near the fjord (Beaird et al., 2017; Hopwood et al., 2025), their fate across a broader spatial and seasonal scale in the bay remains unclear.~~

This study ~~presents~~ addresses these gaps by presenting oceanographic observations spanning two annual cycles from June 2022 to ~~October 2024, supplemented by a regional survey conducted in the summer of 2018.~~ November 2024. These observations provide new insights into the seasonal processes shaping Disko Bay's hydrography and ~~how its waters respond~~ its response to external forcing~~on seasonal timescales. We analyse these observations to shed light on the following three questions: 1) How does the hydrography within the bay evolve throughout the year? 2) What spatial patterns can be observed inside the bay? 3) What local or external processes drive the observed seasonal and spatial variability?~~ , particularly during the poorly observed autumn-to-spring transition

2 Regional setting

The regional circulation in Baffin Bay consists of ~~three~~ two major currents: the northward-flowing West Greenland Current (WGC) and ~~West Greenland Coastal Current (WGCC), as well as~~ the southward-flowing Baffin Island Current (BIC) (Fig. 1a). The WGC carries warm and saline subsurface waters of North Atlantic origin along the continental shelfbreak of ~~West~~ west Greenland (Pacini et al., 2020; Huang et al., 2024). ~~Most~~ While most of these warm waters divert west and south in the northern Labrador Sea, ~~but some continue north past the~~ some continue northward through Davis Strait into Baffin Bay (Cuny et al., 2005; Curry et al., 2011, 2014). Upon crossing the Davis Strait, the warm waters subduct below fresher and colder Polar-origin waters and ~~continue propagating north as a bottom intensified~~ propagate northward as a bottom-intensified current along the continental slope (Huang et al., 2024). Despite the heat loss caused by mixing with the ~~polar water above, the~~ Polar-origin waters above, these subsurface warm waters remain the predominant heat source and ~~cause~~ a major driver of accelerated melt of many ~~of the~~ marine-terminating glaciers along ~~West Greenland (Holland et al., 2008; Straneo et al., 2012; Khazendar et al., 2~~ the west Greenland coast (Holland et al., 2008; Straneo et al., 2012; Khazendar et al., 2019; Joughin et al., 2020; Wood et al., 2021) .

~~Inshore of the WGC, the WGCC carries the freshest waters along the Greenland Coast, consisting of meltwaters from the Arctic Ocean and Greenland Ice Sheet (Fig. 1a) (Foukal and Pickart, 2023). These waters travel south along the East Greenland coast , around Cape Farewell, and then propagate northward towards the Davis Strait (Gou et al., 2022; Foukal and Pickart, 2023) . North of the Davis Strait, the location and fate of WGCC are less clear due to meandering and spatial variability that is hard to resolve (Huang et al., 2024).~~

~~Topography modulates the~~ The exchange of waters between Baffin Bay and Disko Bay ~~. A 300-900~~is strongly modulated by topography. A 300–900 m deep trough~~called~~ , Egedesminde Dyb (ED), cuts across the continental shelf ~~, allowing dense and~~ and provides a pathway for dense, warm waters from the shelf break ~~to enter~~ into Disko Bay (Fig. 1a). ~~However, the passage of these warm waters is~~ This inflow is partially obstructed by Egedesminde Dyb Sill (EDS), ~~which extends to~~ a topographic barrier reaching 300 m depth ~~and creates a barrier similar~~ that functions similarly to a fjord sill (Fig. 1b) (Gladish et al., 2015a). We view EDS as the western boundary of Disko Bay and the approximate delineation of the Disko ~~Bay - Baffin Bay~~ Bay–Baffin Bay boundary. The coast defines the eastern and southern boundaries. In the east, Disko Bay ~~exchanges waters~~ connects with Ilulissat Icefjord (~~750-800~~750–800 m deep), ~~where~~ which is separated by a shallow sill (deepest point of 245 m), also ~~referred~~

~~to~~ known as the Iceberg Bank ~~, separates the two~~ (Gladish et al., 2015b; Morlighem et al., 2022). Disko Island is located in the north of the bay, separated from the mainland ~~to the east by Vaigat Strait. Shallow~~ by the Vaigat Strait (Sullorsuaq Strait), where a shallow bathymetry (245 m) ~~separates Disko Bay and Vaigat Strait~~ also restricts exchange (Andersen, 1981a; Morlighem et al., 2022). Thus, Disko Bay (100 km wide and ∼120 km long) is confined by shallow and complex bathymetry~~and its deepest central area (300-500 m) is~~ , with its central basin (300–500 m deep) isolated from direct water mass exchanges.

Previous studies indicate ~~generally~~ a cyclonic circulation within ~~the bay~~ Disko Bay (Andersen, 1981a; Sloth and Buch, 1984), following ~~the bathymetry~~ bathymetric contours, with northward flow past Ilulissat Icefjord (Beaird et al., 2017), and outflow ~~out of the bay via~~ primarily through Vaigat Strait and along the ~~south~~ southern coast of Disko Island (Andersen, 1981a; Hansen et al., 2012).

3 Data and methods

3.1 Oceanographic observations

We ~~use a combination of~~ combine new observations from two drifting profilers and a hydrographic field campaign ~~, together~~ with existing data from the monitoring station in Disko Bay ~~,~~ to construct a hydrographic time series for ~~2022-2024.~~2022–2024 (Fig.2). Table 1 gives an overview of all hydrographic profiles ~~that make up the 2022-2024~~ included in the time series, and profile locations are shown in Fig. 1b. Additionally, we utilise profiles from ~~two hydrographic surveys in 2018~~ five hydrographic surveys between 2022 and 2024 for a spatial analysis. ~~Below, we describe each dataset.~~

3.1.1 Monitoring ~~station~~Station

We use hydrographic data from the Greenland Ecosystem Monitoring Programme (GEM), ~~which conducts observations~~ collected on board RV *Porsild* at ~~an~~ a fixed oceanographic monitoring station in northwestern Disko Bay (Table 1, Fig. 1b, Greenland Ecosystem Monitoring (2025a)). We obtained all available processed ~~observations from GEM monitoring station between June 2022 and November 2023, which were taken with~~ profiles, taken with a Sea-Bird SBE 19plus instrument ~~with nominal accuracies of ± 0.005°C for temperature, ± 0.005 mS cm^{-1} for conductivity and 0.1% of full-scale range for pressure~~from June 2022 to November 2023, and with an AML Oceanographic AML-6 instrument from May to November 2024. Instrument accuracies are given in Table 1.

~~In addition, we~~ To improve temporal resolution during the undersampled autumn period, we also conducted weekly measurements at the monitoring station from RV *Porsild* ~~throughout the autumn of~~ between August and November 2023 (Table 1, Fig. 1b). ~~We aimed to supplement the GEM profiles over 2023 with higher temporal resolution, targeting the undersampled autumn period. We measured temperature, conductivity, and pressure~~ , using the same Sea-Bird SBE 19plus instrument as ~~used in~~ GEM. We processed the raw data using Sea-Bird Scientific's SBE Data Processing (v7.26.7) application~~and~~ , following standard quality control, correction, and processing steps. ~~Similarly~~In addition, one profile was taken in March 2023 at the landfast

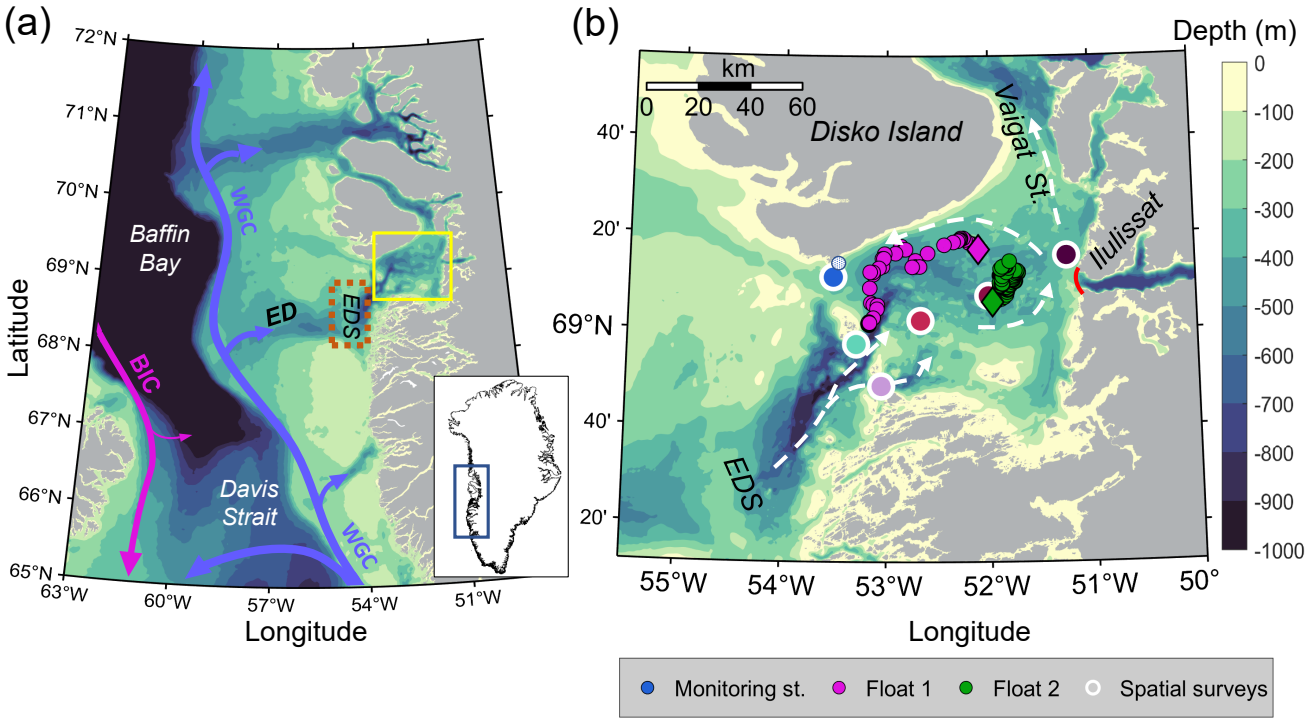

Figure 1. (a) Baffin Bay and ~~West~~ west Greenland bathymetry, overlaid with north-flowing West Greenland Current (WGC, blue) ~~, West Greenland Coastal Current (WGCC, purple)~~ and south-flowing Baffin Island Current (BIC, pink). The Egedesminde Dyb trough (ED) cuts across the continental shelf ~~, entering~~ into Disko Bay (yellow box). The shallow Egedesminde Dyb Sill (EDS) is where we analyse wind forcing with ERA5 reanalysis data (orange ~~dotted~~ dashed box). (b) Disko Bay bathymetry, Ilulissat Icefjord Sill (red line) and general circulation (white arrows, adapted from Hansen et al. (2012)). Location of oceanographic observations: ~~monitoring station~~ Monitoring Station (blue circle with white outline), profile ~~taken~~ from landfast sea-ice (white circle with blue outline), Float 1 (Aug ~~2022 - June~~ 2022–June 2023, ~~pink~~ magenta circles)~~and~~, Float 2 (Aug ~~2023-Oct~~ 2023–Oct 2024, green circles), and stations surveyed during spatial cruises (coloured circles with thick while outline, including the Monitoring Station). Each float's first profile is marked with a ~~cross~~diamond. Bathymetric data are from BedMachine Version 5 dataset (Morlighem et al., 2022).

sea-ice edge, located 2.8 km landward from the monitoring station (Table 1, Fig. 1b)~~, 2.8km landward from the monitoring station~~.

We combined our field observations ~~from this monitoring station~~ (including the profile taken from sea ice) ~~and the~~ with GEM
125 data to construct a spatially fixed time series, ~~which we refer~~ hereafter referred to as "Monitoring ~~station~~Station" ~~.~~ (Fig.2a,c). We use TEOS10 Gibbs-Sea Water Oceanographic Toolbox (McDougall and Barker, 2011) to convert conductivity to Absolute Salinity (S_A), temperature to Conservative Temperature (~~CT~~Θ), and pressure to depth. Throughout this ~~manuscript~~paper, we refer to Absolute Salinity and Conservative Temperature as salinity and temperature, respectively. Hereafter, we refer to potential density anomaly with a reference pressure of 0 dbar (σ_0) as density.

3.1.2 Profiling float data

We use temperature and salinity profiles from an Air-Launched Autonomous Micro Observer (Alamo) float (ID: F9313), deployed in Disko Bay as part of the NASA Oceans Melting Greenland (OMG) Mission (Table 1,Oceans Melting Greenland (2022)). The float ~~followed the general circulation~~ drifted cyclonically within the bay at a mean speed of 0.4 cm s^{-1}, with a higher mean of 0.75 cm s^{-1} while drifting westward before turning south and slowing (Fig. 1b). Between ~~the 6th of February and the 4th of April ,~~ 6 February and 4 April 2023, the float ~~was profiling~~ profiled underneath the sea ice, and ~~no information about the float's position~~ position data during that period ~~is available~~were unavailable. However, between the acquisitions with known positions, the float's position changed only by 3.1 km. The float data ~~was~~ were quality controlled following the recommended procedures in Wong et al. (2024). Hereafter, we refer to this profiling float as ~~Float 1.~~"Float 1" (Fig.2b,d).

Additional profiles were retrieved by an Apex float (WMO ID: 6990591) (Argo, 2024), deployed in Disko Bay in August 2023 as part of the Greenland Ocean Observations (GOO) project (Table 1, Fig. 1b). The data ~~is~~ are Real-time and quality-controlled. We use only the data with a "good data" quality flag and follow ~~up with~~ the same quality control checks and processing as for Float 1.

~~Both Float 1 and~~ Hereafter, we refer to this profiling float as "Float 2" (Fig.2b,d).

Both floats were fitted with RBR sensors ~~with nominal accuracies of ± 0.002°C for temperature, ± 0.003 mS cm^{-1} for conductivity and ± 1 dbar for pressure~~(Table 1). Salinity obtained from both floats was compared against CTD observations ~~to check for possible~~ collected at the Monitoring Station during periods of temporal overlap, and against data from the hydrographic surveys (Section 3.1.3). These comparisons confirmed that the Θ-S_A relationship at higher densities exhibits spatial heterogeneity across Disko Bay (see Section 4.2). Accordingly, float salinities in these density ranges were compared against the full set of available CTD observations in Θ-S_A space, from which we estimate that salinity sensor drift ~~, which was estimated to be less than~~ did not exceed 0.02 PSU over the ~~span of operation of~~ period of data used from either float.

3.1.3 ~~Hydrographic surveys in 2018~~

~~We utilised data from two~~

3.1.3 Spatial hydrographic surveys in 2022–2024

We use data from five hydrographic surveys conducted in ~~the summer of 2018~~ Disko Bay during the summers of 2022, 2023 and 2024 (Table 1, Fig. ~~??~~a) ~~, which we used~~ 1b) to analyse the spatial variability ~~in the bay during the summer months~~during this period. These near-synoptic cruises were conducted as part of the GEM programme (Greenland Ecosystem Monitoring, 2025b), covering most of Disko Bay's deep basin~~and using the same instrument as for the monitoring station observations. The first cruise was conducted on the 27-30th of May (Fig. ??a),~~ . Instrumentation was consistent with the Monitoring Station observations: a Sea-Bird SBE 19plus in 2022 and ~~the second one was from the 30th of August to the 1st of September 2018 (~~2023, and an AML Oceanographic AML-6 in 2024. The cruises took place on 18–21 August 2022, 9–12 May and

Table 1. Overview of analysed hydrographic observations.

Name	Period	Location	Profiles	Sampling ~~frequency~~ freq.	Instrument	Operated by
Monitoring ~~station~~ St.	Jun ~~2022 to Nov 2023~~ 2022–Nov 2024	69° 10’N 53° 31’W	~~16~~ 23	monthly	SBE 19plus[a] / AML-6[b]	GEM
~~Monitoring station~~ Monitoring St.	~~Aug to Nov~~ Aug–Nov 2023	69° 10’N 53° 31’W	6	weekly	SBE 19plus[a]	fieldwork
~~Monitoring station (from sea-ice~~Monitoring St. (sea ice)	Mar 2023	69° 12’N 53° 31’W	1	once	SBE 19plus[a]	fieldwork
Float 1	Aug ~~2022 to Jun~~ 2022–Jun 2023	~~Trajectory~~ see Fig. 1b (trajectory)	63	5-day ~~interval~~ (from 22 Sep 2022)	RBR[c]	NASA OMG
Float 2	Aug ~~2023 to Oct~~ 2023–Oct 2024	~~Trajectory~~ see Fig. 1b (trajectory)	74	5-day ~~interval~~ (from 17 Oct 2023)	RBR[c]	GOO
Hydrographic surveys	~~May, Aug 2018~~ Aug 2022; May & Aug 2023–2024	~~Marked in~~ Fig. ~~??a~~ 1b (stations)	~~37, 20~~ 6 per survey	near-synoptic	SBE 19plus[a] / AML-6[b]	GEM

[a] Sea-Bird SBE 19plus (T: ±0.005 °C; C: ±0.005 mS cm^{-1}; P: 0.1% FS). [b] AML-6 (T: ±0.005 °C; C: ±0.01 mS cm^{-1}; P: 0.05% FS). [c] RBR sensors (T: ±0.002 °C; C: ±0.003 mS cm^{-1}; P: ±1 dbar).

Note: At the Monitoring Station and in hydrographic surveys, SBE 19plus was used in 2022–2023 and AML-6 in 2024.

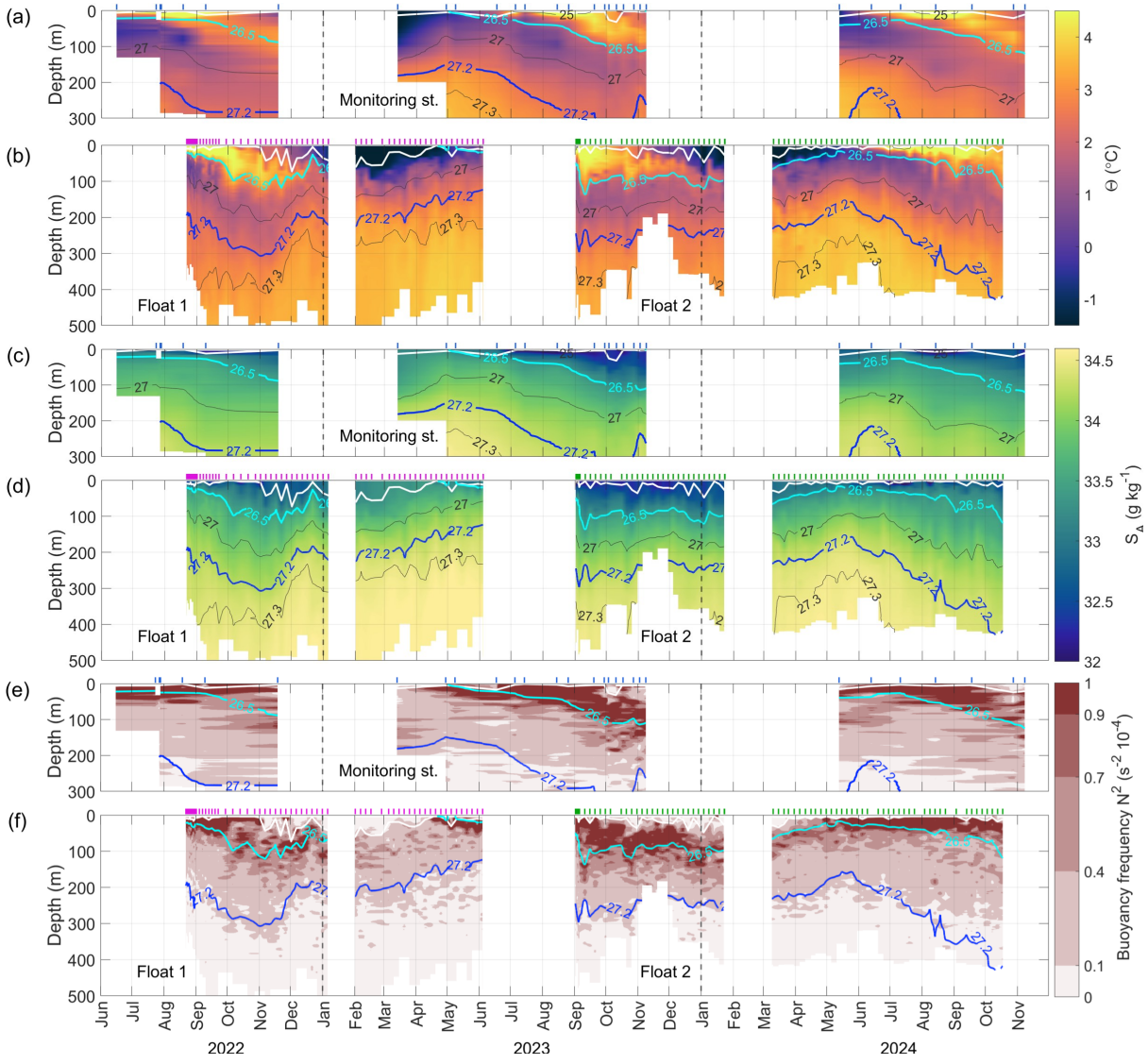

Figure 2. Hydrography in Disko Bay from June 2022 to November 2024. Temperature for the Monitoring Station (a) and profiling floats (b). Salinity for the Monitoring Station (c) and profiling floats (d). Buoyancy frequency for the Monitoring Station (e) and profiling floats (f). Temperature, Salinity, and Buoyancy Frequency are overlaid by labelled isopycnals (blue thick line σ_0= 27.2 kg m^{-3} showing the upper WGIW boundary) and mixed-layer depth (white lines). Vertical ticks on the upper x-axis in panels (a–f) show the time of profile acquisitions (blue –Monitoring Station, magenta – Float 1, green – Float 2), while dashed vertical lines through all panels mark the start of each calendar year.

14–16 August 2023, as well as 16–19 May and 21–22 August 2024. All cruises had the same sampling locations marked in Fig. ~~??a)~~1b.

3.2 Atmospheric and sea-ice data

To estimate atmospheric forcing on local ocean variability in Disko Bay and across the shelf region, we ~~used~~ use the European Centre for Medium-Range Weather Forecasts ERA5 reanalysis product (Hersbach et al., 2023). The product has 0.25° spatial and hourly temporal resolution. We ~~obtain~~ obtained sea-ice concentration and 10-m u and v wind components over a region covering EDS (Fig.1a).

For ~~the~~ sea-ice concentration inside Disko Bay, we use ~~sea-ice concentration (SIC) from~~ data from the merged MODIS-AMSR2 satellite product (Ludwig et al., 2020). Daily ~~SIC~~ sea-ice concentration (SIC) with 1km resolution was downloaded for the Disko Bay region (68°42'N ~~–~~ 69°31'N, 51°24'W ~~–~~ 53°W) and averaged spatially to obtain a time series of weekly mean ~~sea-ice concentration~~SIC.

3.3 Methods

3.3.1 Determination of the mixed-layer depth

~~Based on the calculated density, we determine~~ We determined the mixed-layer depth (MLD) for each hydrographic profile ~~. We find MLD~~ using the two-step method ~~outlined in Semper et al. (2024)~~of Semper et al. (2024), adapted for use with density profiles. First, for each profile, we obtained the preliminary MLD ~~is computed from density profiles. We compute~~ by computing the normalised sum-of-squared errors ~~of densities from the surface down to all possible depth combinations. When a sharp increase in normalised sum-of-squared errors occurs, we detect the depth of the mixed-layer (MLD). We then inspect each profile and confirm that~~ (SSE) over all possible surface-to-depth ranges. Within the mixed layer, normalised SSE values remained small but increased once stratified waters were included as the depth range was extended below the mixed layer. The preliminary MLD was taken as the maximum depth for which normalised SSE values stayed below the threshold of 1.5×10^{-4} kg^2 m^{-6}. In some cases, no MLD was detected, either because the mixed layer was shallower than the first available measurement depth or because no well-mixed surface layer was present.

Second, we verified the preliminary MLD by checking whether temperature, salinity, and density ~~between the surface and calculated MLD fall~~ from the surface to the computed MLD lay within one standard deviation ~~envelope (Pickart et al., 2002; Semper et al., 2~~ of their respective mean values (Pickart et al., 2002; Semper et al., 2024). In a small number of profiles where one or more properties fell outside the standard deviation envelope, the MLD was manually reassigned to satisfy this criterion.

3.3.2 Water mass definitions

Two water masses broadly describe the vertical structure of Disko Bay: a relatively cool and fresh layer of Arctic origin (~~blue shading~~ solid lines in Fig. 3~~b~~d-e), which overlays warmer and more saline waters of Atlantic origin (~~red shading~~ dashed lines in Fig. 3~~b~~d-e).

The ~~Arctic- and the~~ Atlantic-origin waters ~~found in Baffin Bay and the vicinity of Disko Bay have been referred to by several names. The Atlantic-origin waters~~ in the region are often called Modified Irminger Water (Gladish et al., 2015a),

Subpolar Mode Water (Rysgaard et al., 2020), Atlantic Water (Beaird et al., 2017) and West Greenland Irminger Water (Curry et al., 2014; Carroll et al., 2018; Huang et al., 2024). These definitions broadly overlap~~in the properties they describe, and all point to the subtropical Atlantic origin of the warmest waters found along West Greenland. We~~ , and we refer to this water mass as West Greenland Irminger Water (WGIW~~,~~) and define it as waters with a density $\sigma_0 > 27.2$ kg m^{-3} (thick grey isopycnal in Fig. 3~~a).~~ a-c). This definition matches the properties presented by Curry et al. (2014) and those found to be relevant for Disko Bay and Ilulissat Icefjord basin exchanges (Gladish et al., 2015a, b).

~~Similarly, the cool and fresh waters found on the West Greenland shelf~~ The Arctic-origin waters have also been ~~termed differently, referring to a different origin of these waters or their formation process. For example,~~ described using multiple names, depending on origin and formation processes: West Greenland Shelf Water and Arctic Water (Curry et al., 2014; Carroll et al., 2018), Baffin Bay Polar Water and Coastal Water (Rysgaard et al., 2020), cold Polar Water and warm Polar Water (Huang et al., 2024). ~~Most studies looked at near-synoptic data covering large areas of Baffin Bay to delineate these water masses. In this study, we do not differentiate between the origins of the Arctic-origin water inside Disko Bay. Instead, we focus on the seasonal transformations within the present cool and fresh water mass over a given year, and thus,~~ Because we focus on seasonal evolution rather than source differentiation, we use the ~~more~~ general term Polar Water (PW~~, Fig. 3a~~), similar to Myers and Ribergaard (2013), Beaird et al. (2017) and Muilwijk et al. (2022).

~~Hence, we maintain a simple two-layer structure definition for our study: West Greenland Irminger Water (WGIW) and Polar Water (PW). We define WGIW in Disko Bay as waters with a density $\sigma_0 > 27.2$ kg m^{-3}(thick isopycnal line in Fig. 3), matching the properties presented by Curry et al. (2014) and those found to be important in the exchange between Disko Bay and Ilulissat Icefjord basin (Gladish et al., 2015a, b). The lighter~~ The PW has density $\sigma_0 < 27.2$ kg m^{-3}. Through this paper, we also refer to the surface layer, which is defined as the extent of the mixed layer found within PW. We emphasise that this PW definition merges waters from distinct sources into a single, cool and fresh layer. This simplification is necessary as distinguishing individual water mass sources/types is challenging with the data used in this study. Although each of the water types within our PW definition may have distinct origins and seasonal behaviours, we will assess their combined effect on the upper-layer hydrography in Disko Bay.

~~Freshwater fluxes are a vital driver of spatial and seasonal variability in Disko Bay, considering the significant glacial influence in the region (Mernild et al., 2015; Enderlin et al., 2016; Beaird et al., 2017). The major glacial freshwater inputcomes~~ Glacial freshwater input, a significant component of what we term PW in Disko Bay, primarily originates from Ilulissat Icefjord~~,~~ ~~where freshwater fluxes can be partitioned into~~ . This includes both liquid and solid ~~components (Mernild et al., 2015; Enderlin et al., 2016; . A striking feature of the Ilulissat Icefjord is its abundance of icebergs. Icebergs are responsible for most of the freshwater flux at the terminus of Sermeq Kujalleq (Gladish et al., 2015b; Enderlin et al., 2016), representing the solid freshwater component. Icebergs drift and melt as they cross the fjord and the sill into the bay. Thus, when melting, icebergs transition from solid to liquid freshwater flux.~~

~~The liquid freshwater fluxes are~~ fluxes, with the liquid component consisting of runoff and Submarine Melt Water (SMW~~, Fig. 3a) . SMW is formed when~~) (Mernild et al., 2015; Enderlin et al., 2016; Beaird et al., 2017). SMW forms through direct melting of marine-terminating glaciers ~~(or icebergs) melt directly from the heat supplied by the ocean~~ or icebergs by ocean heat

(Θ = -90°C, S_A = 0 g kg^{-1}) (Gade, 1979). Runoff~~is the~~ , from surface melt of glaciers and snow, ~~which commonly~~ typically enters the fjord at depth ~~since runoff percolates into glacial crevasses and drainage channels, entering the fjord at the glacier's base (Straneo and Cenedese, 2015). Runoff that enters the fjord this way is termed~~ via subglacial pathways, forming Subglacial Discharge (SGD, Θ = 0°C, S_A = 0 g kg^{-1}~~, Fig. 3a))~~(Straneo and Cenedese, 2015). Together, SGD and SMW drive convective upwelling ~~inside~~ in the fjord, ~~mixing and entraining the ambient waters at depth and bringing them upwards in the fjord's water column. The final product,~~ entraining ambient waters and producing Glacially Modified Water (GMW~~- mixture of ambient waters, SGD, and SMW, Fig. 3a) equilibrates at the~~) (Straneo et al., 2011; Beaird et al., 2015; Stevens et al., 2016; Beaird et al., 2018; Mor . The GMW equilibrates at its level of neutral buoyancy ~~within the fjord (Muilwijk et al., 2022)~~(Jackson et al., 2017; Cowton et al., 2015; M and is exported into Disko Bay if it extends above the Ilulissat Icefjord sill depth (Jenkins, 2011; Gladish et al., 2015b; Carroll et al., 2016; H .

3.3.3 Wind stress and Ekman pumping calculation

Zonal wind stress (τ_x) and meridional wind stress (τ_y) are computed for each grid point of the ERA5 fields of u_{10} and v_{10} wind speed components ~~. We consider the impact of sea ice on wind stress by incorporating ERA5 sea-ice concentration (A) to obtain the 10-m neutral drag coefficientC_{dn10} following Lüpkes and Birnbaum (2005) parametrisation~~

$$C_{dn10} = (1-A)C_{d,w} + AC_{d,i} + C_{d,f}$$

as follows:

$$\tau_x = \rho_a C_d u_{10} U_{10}, \tau_y = \rho_a C_d v_{10} U_{10} \quad (1)$$

where ~~$C_{d,i}$ and $C_{d,w}$ are the skin drag coefficients over sea ice and open water, for which we used $C_{d,i} = 1.89 \cdot 10^{-}3$ and $C_{d,w} = 1.25 \cdot 10^{-}3$ as in Lüpkes and Birnbaum (2005). The form drag coefficient, $C_{d,f}$, is estimated as~~

$$C_{d,f} = 0.34A^2 \frac{(1-A)^{0.8} + 0.5(1-0.5A)^2}{\alpha_r + 90A}$$

~~where α_r is the aspect ratio D_i/h_f of mean floe length (D_i) to mean freeboard (h_f), which can also be estimated from A as~~

$$h_f = 0.49[1.0 - exp(-5.9A)]$$

$$D_i = 31h_f/(1-A)$$

ρ_a is air density (1025 kg m^{-3}), $U_{10} = \sqrt{u_{10}^2 + v_{10}^2}$ is the magnitude of the wind vector, and C_d is the drag coefficient. To incorporate the effect of sea ice on the surface wind stress, we use a parameterisation $C_D = C_d(A)$, where A is sea ice concentration (Lüpkes and Birnbaum, 2005). The Ekman pumping velocity (W_{Ek}) is then calculated with the curl of the surface wind stress as

$$W_{Ek} = \frac{1}{\rho_0 f_0}\left(\frac{\partial \tau_y}{\partial x} - \frac{\partial \tau_x}{\partial y}\right) \quad (2)$$

where f_0 is Coriolis parameter calculated for each ~~grid cell~~latitude, ρ_0= 1027.0 kg m^{-3} is a reference density and ∂x and ∂y are grid ~~width and height~~size.

4 Results

4.1 Water masses

The two principal water masses ~~can be identified from~~ are evident in the Temperature–Salinity (Θ–S_A) diagrams from the Monitoring Station and Floats (Fig. 3~~a-b, which present all the observations used in this study~~a–c). At the surface, ~~within the mixed layer, PW temperature ranges from~~ PW varies strongly over the seasonal cycle, with temperatures ranging from the in situ freezing ~~temperature to a maximum of~~ point in winter to $\sim$ 8°C ~~during~~ in summer (Fig. 3~~a, b) . Mixing with various freshwater sources lowers the surface salinity to~~ a–c, d) and salinity ranging from $\sim$ 31 g kg^{-1} in summer ~~. During the winter, sea-ice formation and brine rejection increase the surface salinity to a range of 33-33~~to 33–33.4 g kg^{-1} ~~. The PW below the mixed layer exhibits a similarly~~ in winter and early spring (Fig. 3a–c, e).

Between 50 m depth and the WGIW boundary, PW maintains a broad temperature range ~~, spanning from (~~$\sim$ 0 to 4°C~~. It reaches the coldest~~), with the coldest subsurface temperatures in winter ~~alongside mixed-layer deepening and cooling.Once the sea ice melts, the~~ and early spring (Fig. 3b–c, d). After sea-ice melt, surface waters re-stratify and warm~~due to solar insulation. The PW below then forms~~ , while subsurface PW retains a characteristic temperature minimum~~in the water column (seen in the average profile in~~ . This minimum is most pronounced in summer and persists at greater depths in autumn (Fig. 3d).

Mixing with other water sources accounts for the wide property range of PW. Fresh meltwater pulls the near-surface observations along the runoff line in spring (Fig. 3a–c). Similarly, early autumn observations align with the runoff line, while later in autumn they shift toward the SMW mixing line (Fig. 3~~b). The WGIW, characterised by~~ a–c).

In contrast, WGIW ($\sigma_0 > 27.2$ kg m^{-3}~~, ranges from 2 — 4°C and reaches~~) shows less temporal variability, with temperatures of 2–4°C and salinity near $\sim$ 34.6 g kg^{-1} ~~in salinity, showing less variability compared to PW~~ (Fig. 3~~a,b~~a–e).

~~The observations are also presented as time series in~~

4.2 Spatial variability

The five near-synoptic GEM cruises (summers 2022–2024), together with overlapping Float 1 and 2 profiles, reveal significant spatial variability in PW properties across Disko Bay (Fig. ~~2. The observations collected at the monitoring station closely~~

~~match those obtained by the floats during the periods of overlap, confirming the reliability of our approach in combining these sources. Additionally, there is a consistent temporal pattern in the hydrographic development across both years and all observational platforms, suggesting the presence of a seasonal cycle that we will examine in further detail.~~ 4). This variability is especially pronounced in August, with differences of up to 3°C along isopycnals in the $\sigma_0 < 27.1$ kg m^{-3} range (Fig. 4b, d, f). In all August cruises, the coldest upper layer consistently occurred north of Ilulissat Icefjord, while the southwestern region near Aasiaat exhibited a notably warmer subsurface PW relative to all other areas. The spatial contrasts were most distinct in August 2022 (Fig. 4b), when the southern arm of the trough (near Aasiaat) contained the warmest subsurface PW, the middle arm was slightly cooler, and progressively colder conditions were observed toward the station nearest to the trough, then north of Ilulissat Icefjord, and finally at the Monitoring Station south of Disko Island. The central basin was the coldest area overall, aside from a sharp subsurface temperature minimum at the Monitoring Station.

In addition to along-isopycnal variability, PW also exhibits substantial variability along depth levels, particularly in August. The pattern is consistent with isopycnals sloping downward toward the coast, as previously documented north of Ilulissat Icefjord (Beaird et al., 2017). In the spatial cruises, the same tendency is evident at the near-coastal stations both north of Ilulissat Icefjord and near Aasiaat, where, for example, the σ_0 =26.7 kg m^{-3} isopycnal was more than 60 m deeper than in the central parts of the bay.

In contrast, WGIW exhibits much weaker spatial variability. Near-synoptic observations within WGIW fall along a narrow line in the Θ–S_A space (Fig. 4b–f), indicating minimal variability along isopycnals. Differences are somewhat greater along depth levels, but remain small: the PW–WGIW boundary depth varied by 20–30 m across the bay, and standard deviations in density at fixed depths were relatively small and decreased with depth. The average within-cruise standard deviation was $\sim$0.023 kg m^{-3} at 300 m and $\sim$0.014 kg m^{-3} at 400 m, with slightly larger variability in 2024 (both May and August), compared to 2022 and 2023 (Table 2).

Because floats sampled the deeper parts of the bay, analysis of WGIW seasonality relies largely on float data. These observations can be used to assess WGIW variability along isopycnals with confidence, as well as at depth levels, provided that the variability in time exceeds the background spatial variability noted above. The wide spatial coverage of Float 1 in 2022–2023 is considered acceptable for studying WGIW properties, as that period showed limited spatial variability (Fig. 4b, c; Table 2). In contrast, PW seasonality is better assessed from fixed-point observations at the Monitoring Station, since the pronounced spatial variability in PW would obscure the seasonal patterns if Float data are used.

4.3 ~~Surface mixed layer modifications~~

~~Both~~

4.3 Surface mixed-layer modifications

The MLD, mixed-layer salinity, and mixed-layer temperature ~~have a clear annual cycle that follows a consistent development over the two years~~ all exhibit a consistent annual cycle over the observation period (Fig. 5).

Table 2. Spatial variability of West Greenland Irminger Water (WGIW) across Disko Bay from GEM spatial surveys (2022–2024). Variability is reported as the standard deviation of PW–WGIW boundary depth and density at 300 m and 400 m depth. Values are calculated within each cruise across all stations.

Year	Mean PW–WGIW boundary depth (m)	SD of PW–WGIW boundary depth (m)	σ_0 SD at 300 m (kg m^{-3})	σ_0 SD at 400 m (kg m^{-3})
2022 Aug	243	25	0.0187	0.0132
2023 May	157	29	0.0156	0.0148
2023 Aug	239	24	0.0201	0.0048
2024 May	232	19	0.0262	0.0175
2024 Aug	320	23	0.0343	0.0217

~~Mixed-layer temperature is~~ During winter, mixed-layer temperatures remain at the in situ freezing point ~~, and salinity is at the annual maximum value of 33.4~~(Fig. 5b), while sea-ice formation increases mixed-layer salinity through brine rejection (Fig. 5c). The maximum MLD occurs in winter, reaching 61 m in February 2023 and 48 m in January 2024. Continued sea-ice formation increases mixed-layer salinity to a peak of 30–33.4 g kg^{-1} ~~when the bay is sea-ice covered~~ in March (Fig. 5~~b,c). When~~ c), although enhanced stratification and elevated salinity below the mixed layer limit further deepening (Fig. 2e–f).

As sea ice starts to melt in late April, ~~mixed-layer temperature increases, and we see a drop in salinity. This onset of sea-ice melt in late April~~ the mixed layer warms and freshens. This timing is consistent for both 2023 and 2024 and agrees well with satellite-derived SIC, which ~~then~~ drops below 10% ~~.~~ at that time (Fig. 5b–c). Sea-ice melt ~~reduces the MLD, and this shallow layer (~~establishes a shallow mixed-layer (MLD $<$ 20 m)~~is warmed by solar insulation~~ , which warms rapidly due to solar insolation (Fig. 5~~a,b). As summerprogresses, MLD remains small due to increasing surface freshwater input~~ , which lowers a–b). Through summer, increasing freshwater input lowers mixed-layer salinity by $\sim$2 g kg^{-1}~~. In August/September~~, resulting in either a shallow or absent mixed layer (empty markers in Fig. 5a). By August–September, mixed-layer salinity ~~is at its~~

lowest (31–31reaches its minimum (31–31.4 g kg^{-1})and the temperature at its highest value (8–10, while temperature peaks at 8–10°C). (Fig. 5b,c). Over b–c).

In autumn, the mixed layer cools and deepens, together with accompanied by a gradual increase in salinity. Eventually, the maximum MLD is reached during winter (73m in winter 2022-2023, 48m in 2023-2024), with temperature again reaching the in situ freezing point (Fig. 5a,b). This then allows sea-ice formation and a further increase in salinity through brine rejection (Fig. 5c). returning the system to winter conditions and completing the annual cycle.

4.4 Changes in the Seasonality of Polar Water

4.4.1 Temporal variability

From the time series in Fig. 2 we see that at the start of each At the onset of summer, near-surface salinities are reduced salinity reduces in conjunction with mixed-layer freshening . This creates (Fig. 2c–d), establishing a stratified layer with a core that is bound approximately by the $\sigma_0 = 26.5$ kg m^{-3} isopycnal (Fig. 2e,f). We follow the seasonal development of this surface-intensified layer by plotting the two annual cycles of mean salinity in the upper 150 m (Fig. **??**a), capturing the depth range that this stratified fresh layer (approximated by $\sigma_0 = 26.5$ kg m^{-3} isopycnal) extends over (Fig. **??**b). In both years, e–f). As freshwater input and surface warming intensify, the mean upper 150 m salinity begins to decrease in May-June (Fig. **??**a)alongside a gradual deepening of the stratified layer down to 50m by the end of summer (Fig. **??**b). Later in the year, the stratified layer deepens rapidly down to thickens and extends to greater depths, reaching 50 m by late summer, and rapidly extending to $>$ 100 m at the start of autumn, with salinity continuing to decrease throughout the autumn during autumn (Fig. **??**a,b). This autumn decline in upper 150 m salinity continues after the mixed-layer salinities reached their minimum in late August. Overall, the PW salinity over the upper 150 m shows an annual cycle with an amplitude of 2e–f). Although both the Floats and the Monitoring Station capture this seasonal evolution, we assess PW seasonality primarily from the three-year Monitoring Station observations to avoid conflating the substantial spatial variability in PW that Floats would capture (Section 4.2).

The mean salinity of the upper 120 m, encompassing the depth range of the stratified fresh layer ($\sigma_0 < 26.5$ kg m^{-3}), shows a recurring seasonal reduction beginning in June (2023) or July (2022, 2024) and continuing until Monitoring Station observations end in November (Fig. 6a). The magnitude of the summer–autumn freshening varies interannually, reaching ~0.80.5 g kg^{-1} in 2022, ~1 g kg^{-1} .

Seasonal cycle of (a) mean salinity in the upper 150m, with one standard deviation shaded in the background, and (b) depth of the $\sigma_0 = 26.5$ kg m^{-3} isopycnal, which approximates the extent of the stratified layer. The seasonal cycles of 2022, 2023, and 2024 are shown with blue, green, and orange markers, respectively. Star markers are for the monitoring station observations, and circles for the Float 1 and 2.

We investigate PW seasonality in more detail by focusing on the stationary observations at the monitoring station to avoid confounding temporal and spatial variability. In in 2023, the monitoring station observations span the entire spring to late-autumn period, making these time series suitable for further analysis. From monitoring station time series, we saw the

aforementioned seasonal development, with a fresh stratified subsurface layer confined to the upper 50m during summer and its deepening at the start of September (Fig. 2c,f; green star markers in Fig. **??**).

We further examine these changes at the monitoring station with Θ-S_A diagram (Fig. **??**). Alongside freshening in and ~0.6 g kg^{-1} in 2024. Within the $\sigma_0 < 26.5$ kg m^{-3} density range (grey shading in Fig. **??**), temperatures in this density range increased through the summer, peaking in September before beginning to cool over autumn. In contrast, the PW in the $\sigma_0 =$ 26.5-27.1 kg m^{-3} (yellow shading in layer, temperature rises through summer, peaks in August–September, and subsequently cools in autumn while salinity continues to decline (Fig. **??**)continued to warm from September to November. Given that this warming is decoupled from the autumn cooling in the upper layers, we hypothesise that it could be advected. 6a–b).

!htbTheta-SA diagram showing observed temperature and salinity from the monitoring station (blue circle in inset map) spanning June to November 2023 (circle markers coloured by month). Grey contours show isopycnals, with 27.2 kg m^{-3} delineating West Greenland Irminger Water (WGIW) and Polar Water (PW). Grey shading above 26.5 kg m^{-3} marks the isopycnal range where PW is cooling through autumn, while yellow shading marks where along-isopycnal warming occurs simultaneously. The dotted orange line marks the surface freezing point.

4.4.1 Spatial variability in Polar Water across the bay

We investigate the hypothesis that the increasingly warm PW with densities between $\sigma_0 =$ Beneath this layer, denser PW ($\sigma_0 \approx$ 26.5-27.1–27.1 kg m^{-3}is advected towards the monitoring station through autumn (Fig. **??**) . We do that with a spatial analysis by incorporating additional data from two near-synoptic surveys conducted during the summer of 2018) maintains the summer temperature minimum characteristic of PW (Fig. **??**a). These surveys cover much of the deep basin of Disko Bay. We group the observations from May and August into three regions based on bathymetry and a priori knowledge of the general circulation. The regions are defined as eastern, northern, and central (coloured boxes in 3d). In contrast to the lighter PW above (Fig. **??**a). The eastern region is located near the Ilulissat Icefjord, while the northern region follows the outflow path dictated by the bay's bathymetry and circulation. The central region covers the deeper basin of Disko Bay and is thought to be the centre of the cyclonic circulation within the bay. We compare temperature and salinity within these regions and track their changes from May to August 6b), along-isopycnal temperatures within this denser PW layer continue to increase steadily through autumn — rising by 1.6°C in 2022, 1.1°C in 2023, and 0.4°C in 2024 between August and November (Fig. **??**b-d,f-h6c).

In May, the central and northern areas displayed similar hydrographic characteristics (Fig. **??** b-d). However, in the east, the PW temperature gradient was less pronounced (Fig. **??** b) . At depths where other regions exhibited a well-defined PW Θ–S_A space, this steady autumn warming of the denser PW ($\sigma_0 \approx$ 26.5–27.1 kg m^{-3}) appears as a gradual erosion of its sharp summer temperature minimum, the PW in the eastern area was ~0.5°C warmer . Additionally, the upper 25 m in the east were notably fresher and colder than in the other areas with Θ–S_A properties shifting toward warmer values during autumn (Fig. **??** b,c).

By August, all three regions were distinctly different (Fig. **??** f-h). Below the freshened upper layer, the central area maintained a similar hydrographic structure as in May. Its density profile remained largely the same (Fig. **??** h) and a well-defined PW temperature minimum was at the same depths as before (7a–c). Given the strong spatial variability in August

PW properties (Section 4.2; Fig. ?? f). The northern and eastern areas showed more significant changes. In both of these areas, PW had warmed at intermediate depths (50-150m in the east, upper 100m in the north, Fig. ?? 4b, d, f), and there were also changes in salinity and density, with the eastern region showing more significant changes compared to the north (Fig. ?? g, h). The surface layer remained the coldest and freshest in the east(Fig. ?? f, g).

Although there is a temporal development, the overall spatial patterns remain consistent. In the eastern region, near Ilulissat Icefjord, the uppermost layer is notably colder, while the underlying PW is warmer and exhibits a less pronounced temperature minimumcompared to other regions. A similar but weaker pattern is observed in the northern part of the bay. In contrast, the central region remains relatively stable, lacking the pronounced temperature anomalies seen in the eastern and northern regions.

However, comparing properties solely along the depth coordinate provides an incomplete view, as the isopycnals do not lie at the same depths across the bay the warming at the Monitoring Station likely reflects advection from upstream. In August, the station near Aasiaat, in the bay's southwestern corner, consistently had the warmest PW, whereas the Monitoring Station had the coldest PW temperature minimum. When the August Θ–S_A properties from Aasiaat are overlaid onto the Monitoring Station data, the latter's October–November properties closely resemble those observed upstream two to three months earlier (Fig. ?? d,h). Therefore, comparing properties along isopycnals rather than depth offers a more accurate representation. Thus, we calculate the along-isopycnal temperature anomaly in the eastern and northern regions by using the central part of the bay as a reference. We select the central area as a reference for two reasons: first, it is relatively unaffected by the anomalies seen in the east and north, and second, if these anomalies are advective, the centre of the bay lies outside the bay's cyclonic circulation pathway between the east and north. 7a–c), consistent with cyclonic circulation and advection of water masses. The ∼170–200 km distance between Aasiaat and Monitoring Station implies mean velocities of ∼3.3–3.9 cm s^{-1} and ∼2.2–2.6 cm s^{-1} for a two- and three-month lag, respectively.

The results reveal positive along-isopycnal temperature anomalies, especially in the eastern area (Fig. ??e, i). In May, the waters within the $\sigma_0 = 26.75$-27.08 The magnitude of autumn warming at the Monitoring Station along a given isopycnal matches the temperature difference between the Monitoring Station and the Aasiaat station along that same isopycnal in August. For example, along $\sigma_0 = 26.8$ kg m^{-3}density range were ∼0.5, warming from August to November was 1.65°C warmer in the east than in the centre (Fig. ??e). These densities occupy 30-140 m depth in this region (Fig. ??d). A similar anomaly was observed in the northern area within a narrower density range of $\sigma_0 = 26.85$-27.01 kg m^{-3} exhibiting anomalies of ∼0.2°C (Fig. ??e, 30-80 m depth (Fig. ??d)). By August, the warm anomaly in the east extended across a broader density range of $\sigma_0 = 26.32$-27.14 in 2022, 1.1°C in 2023, and 0.48°C in 2024 along $\sigma_0 = 26.8$ kg m^{-3} with the anomaly of ∼0.55°C (Fig. ??i6c). These densities extend to 220 m (Fig. ??h). In the north, densities of $\sigma_0 = 26.29$-27.01 kg m^{-3} displayed similar anomalies of ∼0.4values are comparable to the corresponding along-isopycnal temperature offsets between the Monitoring Station and Aasiaat station in August: 1.89°C in 2022, 1.1°C (Fig. ??i, 30-80 m depth in 2023, and 0.56°C in 2024 (Fig. ??h))7).

In summary, we identify warm along-isopycnal anomalies, indicating that in the east, near Ilulissat Icefjord, waters of the same density are warmer (and consequently more saline) than those in the centre of the bay. From May to August, this

anomaly expanded occupying a broader density and depth range, and increasing in magnitude. A similar trend was observed further north along the outflow path, although over narrower density and depth range, and with a smaller magnitude. The findings suggest that along-isopycnal warming from the east may have propagated towards the northern region. Furthermore, A similar relationship was found only once between the Monitoring Station and the results show a temporal progression of these anomalies between May and Augustwithin the eastern region.

Assuming this spatial pattern is not a transient feature, we can use these results to interpret the along-isopycnal warming within the $\sigma_0 =$ 26.5-27.1 station north of Ilulissat Icefjord. In 2022, denser PW properties at the Monitoring Station in September resembled those north of Ilulissat Icefjord in August. The 1.2°C warming along $\sigma_0 = 26.8$ kg m^{-3} density range observed at the monitoring station in autumn 2023 between August and September at the Monitoring Station (Fig. **??**) . First, we can infer that this signal was likely advected from the east. Then, as spatial analysis showed this signal intensified between May and August 2018 in the east, the continued along-isopycnal warming at the monitoring station in the autumn of 2023 may be reflecting an advective delay.

Expanding this to the entire time series of 2022-2024, we note that along-isopycnal warming in autumn is a seasonal feature 6c) was comparable to the 1.04°C temperature difference between the two locations in August 2022 survey (Fig. **??**). Over the three observed summer-autumn cycles, temperatures at two select deep isopycnals ($\sigma_0 =$26.8 kg m^{-3} and $\sigma_0 =$ 27 kg m^{-3}) showed an increase in autumn. In 2024, the increase in along-isopycnal temperature commenced in August, possibly reflecting the closer proximity of the Float 2 that sampled that year to the eastern region. 7a). The distance of ∼90 km and a 1-month lag yield mean velocities of ∼3.5 cm s^{-1}.

4.5 Seasonality of West Greenland Irminger Water

At depths larger than 300 m, WGIW is isolated within Disko Bay , as it is confined by shallow bathymetric barriers around the bay (200m (245 m at the entrance to Vaigat Strait, 240245 m at Ilulissat Icefjordand 300m at EDS(, 300 m at EDS; Fig.1b)). Regarded as basin water, WGIW can be renewed if equally dense or denser waters pass over the topographic constraints (Gade and Edwards, 1980), with the deepest and most applicable one relevant being the EDS (Gladish et al., 2015a). As such, the (Andersen, 1981a; Gladish et al., 2015a). The onset of a WGIW renewal is seen as characterised by an increase in density below 300 m.

The first signs of WGIW renewal are seen in In early November 2022, when the basin density at 400m began to increase from the m increased from a September-October mean of $\sigma_0\sigma_0(400m)$= 27.31 kg m^{-3} to σ_0= 27.36 kg m^{-3} , reached by early December 2022 (grey shading in November–December in Fig. 8e). Along with this increase in basin density, basin temperatures rose Basin temperatures rose simultaneously by $\sim 0.3°C$ (Fig. 8f). Around two weeks after the basin density began to onset of density increase, the upper boundary of WGIW rose rapidly, with WGIW boundary ($\sigma_0 = 27.2$ kg m^{-3}shoaling) shoaled rapidly by >100 m within a span of two weeks (Fig. 8d), reflecting the uplift of lighter WGIW that previously resided in the basin. Prior to this renewal , This renewal coincided with a seasonal shift in prevailing wind directionoccurred, whereby the along-coast (north-southnorth–south) winds switched from being predominantly southerly in summer to northerly in autumn to spring (from positive wind stress values to negative in Fig. 8b). In the absence of strong sea-ice cover, such northerly

winds (negative wind stress) ~~would lead to~~ drive upwelling over the ~~area of~~ Egedesminde Dyb and its sill (Egedesminde Dyb Sill, EDS). ~~Indeed, upwelling-favourable conditions persisted through~~ Using hourly data, we define "strong upwelling" as $W_E \geq 0.45$ m day^{-1} (upper quartile of the hourly data distribution), typically derived under $\tau_y \leq -0.06\,\mathrm{N\,m^{-2}}$. November 2022 ~~(positive vertical velocity in~~ exceeded these thresholds with $\overline{\tau}_y = -0.1\,\mathrm{N\,m^{-2}}$ and $\overline{W}_E \geq 0.7$ m day^{-1} (Fig. 8~~c), which appears~~ b, c); W_E frequently exceeded $1\,\mathrm{m\,day^{-1}}$ (upper quartile), with episodic peaks approaching $3\,\mathrm{m\,day^{-1}}$. The strength and persistence of this forcing appear to have lifted the dense waters to the west over EDS~~and led to~~, initiating the observed basin renewal in November-December 2022 (Fig. 8~~d~~ f~~d~~–f).

~~In the following months of the winter 2022-2023~~Through winter 2022–2023, basin density ~~did not increase as rapidly as in November and December. Still, a gradual increase from σ_0~~continued to rise gradually from $\sigma_0(400m)$= 27.36 kg m^{-3} to ~~σ_0=~~ 27.39 kg m^{-3} ~~was observed~~ between February and late April ~~2023 (grey shading in~~ (Fig. 8e), ~~indicating a sustained inflow over the EDS. Alongside this increase in density, basin temperatures rose by $\sim 0.5°C$, reaching~~ accompanied by a further $\sim 0.5°C$ increase in basin temperature which reached the annual peak ~~in WGIW temperature~~ at the end of April 2023 (Fig. 8f). This ~~ongoing~~ dense renewal lifted the overlying WGIW, which ~~then~~ continued to rise until ~~the start of June2023 (Fig. 8d) . This period corresponds to the annual maximum vertical extent of WGIW in Disko Bay, with $\sigma_0 = 27.2$ reaching $\sim$100m depth in late May and early June 2023~~ early June, when the upper WGIW boundary ($\sigma_0 = 27.2$ kg m^{-3}) rose to a minimum depth of 120 m (Fig. 8d). Northerly winds ($\overline{\tau}_y = -0.04$ to $-0.07\,\mathrm{N\,m^{-2}}$, upper quartile $\leq -0.12\,\mathrm{N\,m^{-2}}$), Ekman divergence, and positive vertical velocities ~~persisted~~ ($\overline{W}_E = 0.47 - 0.82\,\mathrm{m\,day^{-1}}$, upper quartile $\geq 1.5\,\mathrm{m\,day^{-1}}$) persisted through February–April until the prevailing winds ~~changed direction~~ reversed in mid-May~~2023~~, ending the upwelling-favourable conditions (Fig. 8~~b,c~~b–c).

~~During autumn and winter 2023-2024, basin waters did not increase in density and remained at σ_0= 27.3~~In autumn 2023, the upper WGIW boundary ($\sigma_0 = 27.2$ kg m^{-3}) shoaled by ~50 m in early November (Fig. 8~~e). Northerly~~ d). There were no Float observations deep enough in the basin to document subsequent changes until early winter. However, as neither density nor temperature increased from October 2023 until January 2024, basin renewal likely did not occur. The average wind stress was ~~weaker in September 2023-January 2024 compared to the previous year~~ near zero from September to December, with brief episodes of negative τ_y in October and November (Fig. 8b). ~~Nevertheless, some positive vertical velocities were observed over the EDS area in October-November 2023 (Fig. 8c), coinciding with a slight 50m uplift of the WGIW boundary at the start of November~~ Calculated upwelling velocities were $\overline{W}_E = 0.3\,\mathrm{m\,day^{-1}}$ in October, with short-lived episodes of $W_E > 0.6\,\mathrm{m\,day^{-1}}$ (upper quartile), but overall, the forcing was weaker and less persistent than in November 2022 (Fig. 8~~d). In March and April 2024, signs of renewal were observed, as basin density increased by 0.1~~c).

There are signs of a renewal in March–April 2024, when $\sigma_0(400m)$ increased by 0.01 kg m^{-3} and the temperature rose by ~~approximately $\sim 0.5°C$ over~~ $\sim 0.3°C$ within one month (orange ~~shading~~ shadings in Fig. 8e, f). ~~However, wind forcing and upwelling were not evident during this period, suggesting a non-local mechanism behind this renewal. By the end of May and the start of~~ Lack of observations between 23 January and 11 March hinders the ability to determine when this renewal began; however, density and temperature in the basin were already higher by 0.02 kg m^{-3} and $\sim 0.4°C$ by 11 March, suggesting it was already underway. Winds during January–April were upwelling-favourable ($\overline{\tau}_y$ = -0.01 to 0.05 $\mathrm{N\,m^{-2}}$), with mean

vertical velocities of $0.1 - 0.6\,\mathrm{m\,day^{-1}}$. The strongest forcing (upper quartile) occurred in March with $\tau_y \leq -0.11\,\mathrm{N\,m^{-2}}$ and $W_E \geq 1.1\,\mathrm{m\,day^{-1}}$. By late May – early June 2024, ~~similar to spring 2023, this inflow resulted in the maximum observed vertical extent of WGIW~~ the WGIW boundary rose to a minimum depth of ~150 m (Fig. 8d).

In both years, the ~~WGIW reached its maximum vertical extent in May-June, reaching 150~~upper WGIW boundary was shallowest in May–June, shoaling to 120 m in 2023 and ~~180~~150 m in 2024 (Fig. 8d). This ~~shoaling of the WGIW makes the warm waters available above~~ uplift brought WGIW waters in Disko Bay above 240 m depth, corresponding to the Ilulissat Icefjord sill depth~~(~~. At 240 m ~~). Observations at the same depthin Disko Bay show a seasonal temperature cycle of $\sim 2°C$, with a peak of $> 3.5°C$ in May-June (Fig. 9b). The density at 240 m depth follows a similar seasonal pattern, with a peak of~~ depth, density showed a pronounced seasonal cycle, peaking at σ_0= 27.3-27.35 kg m^{-3} in May ~~/June and a minimum density~~ and declining to a minimum of σ_0= 27.1 kg m^{-3} ~~from August to November~~ in August–November (Fig. 9a). ~~We note that there is a spatial variability around these depths in August-November, previously highlighted in Sect. 4.3.2, which is also seen in a more extensive spread of observed densities and temperatures in the autumn of 2023-2024 cycle~~ Temperature at 240 m varied in parallel, with an amplitude of $\sim 2°C$ and maxima above $3.5°C$ in May–June (Fig. 9~~a~~,b). ~~These observations come from the monitoring station and Float 2 (star and circle markers, respectively, in Fig. 9a,b), thus reflecting the spatial variability. Overall, depending on the basin density in the Ilulissat Icefjord, the densest waters for Ilulissat Icefjord renewal are available in May/June. Additionally, a pronounced autumn WGIW renewal in Disko Bay, similar to the one observed in November-December~~ A renewal event in November–December 2022 ~~, can elevate the WGIW enough to drive a temperature increase of $\sim 1.5°C$ at the Ilulissat Icefjord sill depth~~ resulted in $\sim 1°C$ warming at 240 m (Fig. 9b). ~~This suggests that, at times, warm and dense waters could become available for renewal in the Ilulissat Icefjord as early as late autumn and early winter.~~

5 Discussion

Our results documented two full annual cycles (2022–2024) of hydrographic properties within Disko Bay. ~~In addition to~~ Beyond the expected seasonality ~~within the mixed layer~~in the surface mixed layer (Fig. 5), we observed notable seasonal and spatial variability within PW and ~~seasonal~~ a recurring inflow of dense WGIW that replenishes the deep basin and elevates the WGIW–PW interface. Our results reflect the renewed "warm" state of Disko Bay that has persisted since 2020 (Picton et al., 2025), following the short-lived anomalously cool period of 2015–2019 (Khazendar et al., 2019; Picton et al., 2025). ~~In what follows we discuss the sources of the observed signals and compare them to earlier relevant studies.~~

5.1 ~~Phases of Polar Water seasonality~~

The seasonal cycle of PW ~~and the mixed layer within follow three main phases. First, in winter and spring~~can be divided into three phases: (1) in winter–spring, cooling, sea-ice formation, and brine rejection increase the ~~salinity in~~ density and depth of the mixed layer~~as it deepens (Fig. 5) . Second, ~~; (2) with the onset of ~~summer and~~ the melt season, a ~~shallow and~~ fresh stratified layer develops ~~, isolating PW below, which forms a characteristic temperature minimum in the water column.~~

Finally, at the end of summer and into autumn, PW undergoes counter-intuitive changes. A fresh, stratified layer extends over the upper 150 m , causing isohalines to deepen as autumn progresses in the upper 50 m, bounded by the $\sigma_0 = 26.5$ kg m^{-3} isopycnal (Fig. 2e); and (3) in late summer–autumn, stratified layer ($\sigma_0 < 26.5$ kg m^{-3}) extends over 120 m while freshening and cooling (Fig. **??**). Additionally, throughout autumn, along-isopycnal warming is observed below this stratified, fresh layer (6a–b), while the denser PW beneath ($\sigma_0 \approx 26.5$–27.1 kg m^{-3}) warms steadily along isopycnals (Fig. **??**, 6c; Fig. **??**). Thus, a two-way development in PW occurs in autumn: 1) a fresh, stratified layer that extends deeper and gradually cools and 2) below this , along-isopycnal warming7). In the following sections, we examine the mechanisms driving this autumn evolution of PW before turning to the renewal of WGIW.

While processes occurring in winter, spring, and summer are well understood, those in autumn warrant further discussion.

5.1 Autumn evolution of Polar Water

5.1.1 Remote and local drivers of autumn freshening

5.1.2 Deepening of fresh and stratified layer

One potential source of this deep fresh signal at the start of autumn is lateral advection of upstream waters with the WGC/WGCCBoth remote and local processes can contribute to the autumn freshening observed in the upper 120 m (Fig. 6a) and the associated vertical expansion of the stratified layer (Fig. 2e). The primary remote source is advection of signals from the West Greenland Current (WGC). Observations from the Davis Strait mooring array show a clear annual cycle in salinity, with peak salinities along the west Greenland shelf between April-June April–June (33.66 g kg^{-1}) and a decrease towards the annual minimum in August-October August–October (32.75 g kg^{-1}) (Curry et al., 2014; Carroll et al., 2018). Deeper in the water column, at the Similar seasonality occurs along the shelf-slope at Davis Strait ($\sim$ 150 m) the salinity follows the same annual cycle (Gladish et al., 2015a)(Gladish et al., 2015b). Given that Davis Strait is lies $\sim$ 400 km south of Disko Bay and the subsurface velocity of WGC is around WGC velocity is $\sim$ 0.07m m s^{-1} in autumn (Curry et al., 2014), these signals are expected to could reach Disko Bay with a delay of about two months. This timing aligns well with the observed seasonality in Disko Bay, where we see a fresh signal extending over the upper 150 m at the start of autumn , consistent with the timing of autumn freshening at the Monitoring Station (Fig. **??**),i.e. two months after the onset of decreasing salinities along the shelf.Therefore, the seasonal feature observed in Disko Bay may reflect the influence of freshwater advected by the WGC/WGCC2d,f; Fig. 6a). However, typical minimum density and salinity at $\sim$ 150 m in Davis Strait tends tend to be higher ($\sigma_0 > 27$ kg m^{-3} and $S_A > 33.8$)(Gladish et al., 2015a), compared to what we observe S_A>33.8 g kg^{-1})(Gladish et al., 2015b) than those observed at the same depth in Disko Bay during autumn (Fig. 2c,d). Therefore, an additional source of fresh signals may be more localised c–d), suggesting that local freshwater inputs within Disko Bay likely contribute as well.

The Ilulissat Icefjord significantly contributes to freshwater fluxes, which originate from three primary sources in the fjord. The first source is glacial runoff that enters the fjord at depth as SGD. The other two are the underwater melting of the glacier terminus and melting icebergs, both of which form the SMW component. These freshwater fluxes vary in magnitude seasonally. The most substantial contributor is the melting of icebergs within the fjord, with estimates increasing from 700-1000significant

local source is Sermeq Kujalleq, which delivers large summertime freshwater fluxes through subglacial discharge (SGD, 900 m^3s^{-1} ~~during winter to a peak of 1200-1800~~(Mernild et al., 2015; Enderlin et al., 2016) and submarine meltwater (SMW, 70-400 m^3s^{-1} ~~in August (Enderlin et al., 2016; Kajanto et al., 2023). The second-largest contribution comes from SGD, which has near-zero fluxes in winter that rise to around 900 m~~(Enderlin et al., 2016; Kajanto et al., 2023). A mix of these melt products, together with entrainment of PW and WGIW, forms GMW, whose vertical reach is strongly controlled by SGD seasonality (Cowton et al., 2023; Kajanto et al., 2023; Hager et al., 2024). Icebergs within Ilulissat Icefjord are a dominant freshwater contributor (700–1000 m^3s^{-1} ~~in summer (Mernild et al., 2015; Enderlin et al., 2016). The SMW contribution from terminus melt remains highly uncertain, as it is influenced by seasonal variations in SGD . In the summer, a buoyant plume generated by SGD enhances melting at the terminus, boosting its SMW contribution to a peak of about 70-400~~ in winter, up to 1200–1800 m^3s^{-1} ~~(Enderlin et al., 2016; Kajanto et al., 2023). In winter, with near-zero SGD, terminus melt is similar to that of icebergs. However, since the area of the submerged glacier terminus is at least an order of magnitude smaller than the submerged area of icebergs (9-27 km^2 for the submerged terminus versus 470-690 km^2 for icebergs) , the contribution of SMW from terminus melt is relatively minor in winter (Enderlin et al., 2016).~~

~~A mix of these melt products, PW, and WGIW, forms a new water mass GMW~~in August) (Enderlin et al., 2016; Kajanto et al., 2023) , altering water mass properties within the fjord, modifying the neutral buoyancy depth of GMW, and cooling the fjord basin through reflux of outflowing water (Kajanto et al., 2023; Hager et al., 2024). The GMW ~~that exits from Ilulissat Icefjord into Disko Bay flows north~~ exported from the fjord over the sill flows north in Disko Bay as a buoyant stratified current~~(Beaird et al., 2017). This current features~~ , with a cold, fresh ~~, stratified layer that extends~~ signature extending to at least 100 m ~~deep~~ depth near the shore ~~, as observed in August 2014 by Beaird et al. (2017). They noted that the concentration of meltwater decreased offshore, resulting in a shoaling of the GMW layer ; however, the upper~~ (Beaird et al., 2017). Offshore, this layer shoals to $\sim$ 35~~m retained the cold and fresh GMW~~ m, but retains its signature up to 10 km offshore ~~. We refrain from directly comparing our results from the 2018 cruises with the data from 2014, as the conditions in 2018 were notably different. 2018 was an anomalously cold year in Disko Bay (Khazendar et al., 2019; Joughin et al., 2020); this can be seen when comparing temperature profiles in 2022-2024~~ (Beaird et al., 2017). Our spatial analysis detected similar anomalies each August north of Ilulissat Icefjord (Fig. ~~3b) and 2018 (Fig. ??b,~~ 2b, d, f). ~~However, our results do indicate a similar cold and fresh anomaly in May and August 2018 near the Ilulissat Icefjord. We also observed this anomaly propagating further north and west as it moved downstream. Thus~~Given that the peak melt season in the fjord occurs in July–August (Wood et al., 2025; Picton et al., 2025; Mernild et al., 2015; Enderlin et al., 2016; Kajanto et al., 2023), the export of thick meltwater-laden GMW ~~in the upper layers could be an additional reason for the seasonally observed freshening and deeper extension of the stratified layer at the start of autumn, considering that the peak melt season in the fjord occurs around August.~~could contribute to the freshening observed downstream at the Monitoring Station during autumn. Continued iceberg melt after the melt season (Moon et al., 2018; Kajanto et al., 2023) may also explain why autumn observations in the Θ–S_A diagram aligned with the SMW mixing line (Fig. 3a–c; Fig. 7a–c). While such alignment could reflect inputs of iceberg melt, it might also result coincidentally from autumn cooling, and disentangling these processes would require additional tracers (Beaird et al., 2015, 2018; Lindeman et al., 2024).

Finally, ~~this fresh anomaly may partly be maintained by the continued melting of the icebergs~~ the iceberg melt within Disko Bay ~~, where a high density of icebergs persists year-round (Enderlin et al., 2016; Scheick et al., 2019)~~itself provides an additional but smaller freshwater input. The annual average solid ice discharge at the terminus of Sermeq Kujalleq is ~~around~~ $\sim$ 50~~Gt/yr, which equates~~ Gt yr^{-1}, equivalent to $\sim$ 1500 $m^3 s^{-1}$ (Mankoff et al., 2020). Given that the annual average iceberg melt inside the fjord is $\sim$ 1200 $m^3 s^{-1}$ (Kajanto et al., 2023), ~~it suggests that~~ up to 80% of ~~icebergs may already~~ discharged icebergs likely melt inside Ilulissat Icefjord. The remaining ~~icebergs, however, can cross over~~ fraction can cross the sill and enter Disko Bay~~. Inside Disko Bay, the iceberg size distribution is predominantly made up of smaller icebergs. At times,~~ , where more than 1000 small icebergs (with an area of about 1800 m^2) ~~,~~can be observed simultaneously (Scheick et al., 2019). ~~Assuming an average rectangular~~ To estimate their potential freshwater flux, we represent an average iceberg of this size ~~, its length would be~~ as $\sim$ 130 m ~~, height~~ in length and width. Icebergs in Ilulissat Icefjord are typically twice as wide as they are thick (Enderlin et al., 2016), giving an estimated thickness of $\sim$ 65 m (~~based on aspect ratios of typical icebergs in Ilulissat Icefjord (Enderlin et al., 2016)), and draft~~ freeboard+draft). Using the freeboard-to-draft ratio of 1:7 (Cenedese and Straneo, 2023), we estimate the draft of $\sim$ 55 m~~(Cenedese and Straneo, 2023)~~. Given the average summertime temperature of 2°C in the upper 50 m, and assuming fully turbulent conditions around the iceberg, we estimate that the upper bound of summertime meltwater flux from 1000 of ~~these~~ such icebergs would be around 65 $m^3 s^{-1}$. ~~This indicates that while iceberg melting during summer in the bay is significant, it is not the primary source of freshwater~~While non-negligible, this contribution is small compared to freshwater inputs within Ilulissat Icefjord and therefore unlikely to be the primary driver of the continued autumn freshening observed at the Monitoring Station.

5.1.2 Along-isopycnal warming at depth

~~The glacial influence may also explain the deep warm~~ Beneath the stratified fresh layer, a continued along-isopycnal ~~anomalies we observed , which were most pronounced near Ilulissat Icefjord in 2018 surveys~~ (warming was observed within denser PW ($\sigma_0 \approx$ 26.5–27.1 kg m^{-3}; Fig. ~~?? e,i). Typically, the characteristic warm signature of GMW arises from the entrainment of WGIW, which contributes a significant fraction of the water masses present in the GMW layer , while meltwater (SGD and SMW) remains highly diluted and is not dominant.For example,GMW exported from Ilulissat Icefjord contains about 40% WGIW (Beaird et al., 2017). As a result,GMW is generally warmer and more saline than unmodified water of the same density (Beaird et al., 2018; Muilwijk et al., 2022; Cowton et al., 2023)~~6c; Fig. 7). By October–November, hydrographic properties at the Monitoring Station closely matched those measured near Aasiaat two to three months earlier, suggesting an advective signal that may enter Disko Bay from the southwest and be advected cyclonically around the bay.

A similar late-autumn warming below 150 m was previously documented by Hansen et al. (2012), who attributed it to entrainment of warm surface waters. In our observations, however, the overlying PW layer cools and continues to freshen during this period, while the warming at depth is accompanied by a slight increase in salinity (Fig. 7b,d,f). These features are more consistent with the advection of warmer, saltier water masses than with vertical mixing from the surface.

~~Although we cannot directly quantify the specific contributions of water masses to GMW, the observed anomalies suggest the presence of WGIW at depths typically occupied by PW. A warm along-isopycnal anomaly was observed at depths of~~

30-134 m in May near Ilulisat Icefjord Without hydrographic profiles outside Disko Bay, we cannot definitively establish the sources of this warming before it appears near Aasiaat. However, at depths comparable to those of the $\sigma_0 \approx 26.5$–27.1 kg m^{-3} PW layer in autumn (Fig. ?? d,e), which deepened to 50-220 m by August (Fig. ?? h, i). Since this anomaly occurred at depths shallower than the Ilulissat Icefjord sill, it is possibly sourced from the fjord itself. Similar warm anomalies have been identified in numerous glacial fjords along northwest Greenland (Muilwijk et al., 2022; Cowton et al., 2023) and in southeast Greenland (Beaird et al., 2018). The deepening of this layer from May to August aligns with model results by Cowton et al. (2023), which suggest that as subglacial discharge decreases in late summer and autumn, the GMW plume's neutral buoyancy shifts to greater depths. 2), long-term moorings at Davis Strait record a pronounced seasonal temperature cycle along the west Greenland shelf and slope. Instruments at 151 m and 252 m show temperatures increasing from summer minima to peak values in December-February, while water masses remain least dense during autumn (Gladish et al., 2015b; Carroll et al., 2018). Although mooring records are not yet available for our study period, the warming observed propagating toward the Monitoring Station in autumn may represent the advection of this recurring Davis Strait signal.

If an anomaly exists outside the Glacial processes may also contribute to the observed warming. Buoyant plumes of SGD and SMW drive turbulent upwelling that entrains the warm and saline Atlantic-origin waters, producing GMW that is commonly warmer and more saline than unmodified Polar Water of the same density found at a distance away from the glacier (Straneo et al., 2012; Beaird et al., 2017, 2018; Mortensen et al., 2020; Muilwijk et al., 2022; Cowton et al., 2023). For instance, GMW exported from Ilulissat Icefjord has been estimated to contain about 40% of WGIW (Beaird et al., 2017), making it distinctly warmer and saltier than ambient PW. GMW export from Ilulissat Icefjord , it would circulate Disko Bay following the general cyclonic flow. This is then consistent with a warm anomaly of GMW origin exported from the Ilulissat Icefjord , carried with the cyclonic circulation around the bay at its isopycnic level, and later arriving further downstream (e.g. monitoring station in autumn may therefore enhance autumn anomalies in PW. However, our spatial analysis showed that the highest along-isopycnal temperatures in August occurred further upstream, near Aasiaat (and, in 2023(Fig. ??)). Furthermore, we observed that , within the deep trough entering Disko Bay), rather than near Ilulissat Icefjord. We therefore interpret the autumn along-isopycnal warming was a seasonal feature in all three sampled autumns, indicating that it was not a transient feature (Fig. ??). primarily as the seasonal signal of the WGC, while GMW exported from Ilulissat Icefjord may provide a secondary, but smaller, contribution.

5.2 West Greenland Irminger Water renewal

Our observations over Over two annual cycles (2022-2023, 2023-2024)show that seasonal WGIW renewal occurs in spring. We demonstrate that during spring, 2022–2023, 2023–2024), renewal of WGIW in Disko Bay occurred primarily in spring, when the densest WGIW fills the Disko Bay filled the basin, resulting in maximum temperatureand salinity, as well as the greatest annual maxima in density, temperature, salinity, and vertical extent of WGIW observed throughout the year (Fig. 8d-fd–f). The springtime renewal process begins in February/March and reaches its peak by May/June in both yearsbegan in February–March and lasted until May–June. This provides direct observational evidence supporting the hypothesis proposed by of Gladish et al. (2015a, b), who suggested proposed that exchange over the EDS likely occurs in spring. Indeed, we observed

~~the arrival of the densest WGIW in spring, which has also been observed further north along the West Greenland coast (Carroll et al., 2018)~~This timing also matches observations further north in Uummannaq fjord system (Carroll et al., 2018), and south in Godthåbsfjord (Mortensen et al., 2011, 2014). At 240 m in Disko Bay (Ilulissat Icefjord sill depth equivalent), WGIW density peaks at $\sigma_0 = 27.3$–27.35 kg m^{-3} in May (Fig. 9a), matching the density range observed within Ilulissat Icefjord basin (Gladish et al., 2015b, a; Beaird et al., 2017). This correspondence suggests that spring renewal in Disko Bay delivers the densest waters entering the fjord basin.

The repeated springtime renewal ~~of dense WGIW~~ in Disko Bay ~~aligns with the broader annual WGIW cycle and the vertical isopycnal displacement of about 140m at the shelfbreak in Davis Strait(Curry et al., 2011, 2014; Gladish et al., 2015b; Carroll et al., 2018) . During spring, isopycnals over the West Greenland slope and shelf exhibit an upward tilt~~ is consistent with regional-scale hydrographic variability. At Davis Strait, isopycnals tilt up toward the Greenland shelf ~~, coinciding with densification of WGIW~~ in spring, with ∼140 m vertical displacement of WGIW at the shelfbreak coincident with densification along the shelf ~~that reaches its maximum in April at Davis Strait (Curry et al., 2014; Gladish et al., 2015a). As a result, increasingly dense waters may~~ (Curry et al., 2011, 2014; Gladish et al., 2015b; Carroll et al., 2018). Increasingly dense waters thus become available over the EDS, eventually exceeding the density of resident basin waters in Disko Bay and ~~renewing the basin during spring.~~

~~Our results also suggest that WGIW renewal can occur following periods of~~ driving the springtime renewal (Fig.10b). Persistent upwelling-favourable winds ~~. We observed clear signs of renewal in late autumn of~~ locally through spring likely enhance the renewal process (Fig.8b–c).

In addition to the repeated spring renewal, we observed a distinct renewal in November–December 2022, marked by ~~a rapid increase~~ rapid increases in basin density and temperature ~~, followed by a notable vertical increase in the thickness~~ and a >100 m shoaling of the WGIW ~~layer within the bay~~ boundary (Fig. 8~~d-f~~d–f). This autumn/winter renewal was unique to the ~~2022-2023~~ 2022–2023 annual cycle and coincided with particularly strong and persistent upwelling-favourable winds~~over the EDS area~~. These conditions likely induced upwelling ~~near~~ over the EDS, lifting the dense waters over the ~~topographic constraint and facilitating their access~~ sill and into Disko Bay ~~. We estimated the upwelling velocity during the favorable period to about 1 m day^{-1} or atotal uplift during the period of around 15 m , but the upwelling velocities may be larger than the values obtained using Eq. 5 since EDS is located relatively close to the coast, so that coastal upwelling may play a role. Similarly, Carroll et al. (2018) attributed the increased presence of WGIW~~ (Fig.10a). Estimated vertical velocities frequently exceeded $1\,\mathrm{m\,day^{-1}}$, with episodic peaks approaching $3\,\mathrm{m\,day^{-1}}$, implying uplift on the order of ∼20 m during this period. The actual uplift may have been greater, as our estimates only quantify the effect of wind stress curl, and not coastal upwelling, which could also contribute, given the proximity of the coastline east of EDS.

While we cannot determine the precise magnitude of upwelling or the properties of upwelled waters over the EDS without hydrographic observations on the shelf, the conditions observed are consistent with other studies linking upwelling-favourable winds to WGIW intrusions along the west Greenland shelf. For example, upwelling-favourable winds were linked to the observed increased WGIW presence in the Uummannaq trough ~~, located~~ (300 km north of Disko Bay~~, to upwelling-favourable conditions in Baffin Bay during December-January. Our results indicate that this mechanism of WGIW transport into Disko Bay~~

may increase the density at depths above the Ilulissat Icefjord sill earlier in the year than previously expected (Gladish et al., 2015a, b) .

5.3 The significance of the unravelled seasonality

The enhanced understanding of hydrographic seasonality presented here aids in interpreting long-term time series from Disko Bay , particularly those from continuous monitoring at its northwestern end (GEM monitoring station). A better understanding of the seasonality locally enables the de-seasoning of these time series. Our results also help evaluate the observations in a spatial context. Specifically, we find that waters exported from Ilulissat Icefjord are transported further into the bay by the general circulation, likely reaching as far as the monitoring station. While the lack of velocity observations prevents precise quantification of the advective timescale, we estimate that signals from Ilulissat Icefjord take a few weeks to arrive there.

Since the 2000s, increased meltwater delivery has contributed to higher primary production) during December–January (Carroll et al., 2018), and to modelled areas of frequent upwelling along the coast both north and south of Disko Bay (Ribergaard et al., 2004 . Near Cape Farewell, wind-driven upwelling events have been shown to draw Atlantic-origin waters from $\sim$ 250 m depth onto the shelf ($\sim$ 150 m), raising both temperature and salinity (Pacini and Pickart, 2023). In southeast Greenland, at Sermilik Fjord, along-shelf winds were also shown to play an important role in uplift and onshore intrusion of dense Atlantic Waters (Snow et al., 2023; Sanchez et al., 2024).

Our results highlight that a pronounced autumn/winter WGIW renewal, such as in 2022, can shoal the WGIW boundary enough to increase the temperatures at Ilulissat Icefjord sill depth by $\sim 1°C$ (Fig. 9b). While fjord renewal is primarily driven by SGD during the melt season (Gladish et al., 2015b, a; Carroll et al., 2017), our observations show that episodic autumn/winter uplift of dense waters in Disko Bay , and the upwelling related to glacial processes has been shown to influence coastal phytoplankton dynamics in the bay as far as up to 50 km offshore (Oliver et al., 2023). Nutrients are upwelled and entrained into GMW within Ilulissat Icefjord (Hopwood et al., 2025), and we have described how this watermass spreads out into the bay spatially and seasonally. The nutrients are transported into the Disko Bay and subsequently into Ilulissat Icefjord with the nutrient-rich WGIW, making our findings on WGIW renewal directly relevant to marine biologycan make waters denser than those in the fjord basin available above the sill earlier in the year than previously expected (Gladish et al., 2015a, b) and during periods of limited SGD forcing (Mernild et al., 2015; Enderlin et al., 2016). Observations in Disko Bay reported by Picton et al. (2025) indicate that late autumn–early winter renewal may have taken place in 2021 as well, as temperatures at 240 m increased rapidly by $\sim 0.5°C$.

Finally, an improved understanding of seasonality can provide an important context for interpreting the seasonal phenology of marine organisms within the bay, as well as for modelling and observational efforts to resolve Ilulissat Icefjord dynamics, now and in the futureWe therefore extend the schematic of Gladish et al. (2015a) to include a wind-driven autumn/winter renewal pathway across the EDS into Disko Bay, while also acknowledging the possibility that such events may enable dense inflow into Ilulissat Icefjord basin (Fig.10a), although direct evidence for this process is not yet available.

6 Conclusions

~~This paper examines hydrographic seasonality in Disko Bay using observations from summer 2018 and the June~~

We examined two full annual cycles (June 2022 ~~–October~~ – November 2024~~period. Our findings reveal a consistent seasonal cycle, spanning from the surface mixed layer to deep waters, that governs annual hydrographic variability in the bay. By integrating data from a~~) of Disko Bay hydrography using fixed-point observations from a monitoring station, ~~regional surveys, and~~ two profiling floats, ~~we provide a comprehensive picture of seasonal and regional influences on the bay's hydrography. The interplay between glacial outflow from the east and water-mass exchange from the west varies across space, depth, and time, shaping the bay's hydrography throughout the year~~and near-synoptic surveys to resolve the seasonal evolution and spatial structure of PW and WGIW.

~~Surface layer warming and freshening begin with sea ice melt . A shallow stratified surface layer reaches a maximum of~~ Sea-ice melt initiates a shallow mixed-layer that warms up to ~~8~~ 8–10°C ~~and a salinity minimum of~~ while freshening to ~~31~~ 31–31.4 g kg^{-1} by late summer. Spatially, ~~surface mixed~~ the surface layer varies across the bay, with the coldest and freshest waters found ~~in the vicinity of~~ near Ilulissat Icefjord.

~~The significant seasonal and regional differences within the bay are within Polar Water (PW), also below the mixed layer. PW exhibits a distinct annual salinity cycle of~~ Below, freshwater input establishes a stratified layer bounded by $\sigma_0 \approx 26.5$ kg m^{-3}, which progressively thickens and extends downward from the upper ~~0.8 g kg^{-1}, with decreasing salinity from summer to late autumn. We suggest this signal reflects substantial seasonal freshwater fluxes in the Ilulissat Icefjord and Disko Bay system.~~

~~In addition to salinity variations, autumnalong-isopycnal warming of the PW core is consistent with the influence of Glacially Modified Water (GMW), which reflects the presence of entrained warm WGIW into the buoyant glacial plume. Such glacial influence is most substantial in the east of Disko Bay, where exchange between Disko Bay and Ilulissat Icefjord occurs. We found that this warm along-isopycnal anomaly circulates cyclonicly within the bay~~ 50 m in summer to depths exceeding 100 m in autumn. This layer cools and continues to freshen during autumn. Along isopycnals within denser PW ($\sigma_0 \approx 26.5$–27.1 kg m^{-3}), temperatures steadily increase through autumn. Near-synoptic surveys show that the warmest August PW of such densities occurs upstream at the southwestern end of the bay, and ~~propagates along the outflow path~~that Monitoring Station properties in October–November match those found upstream with a 2–3 month delay, consistent with cyclonic advection around the bay. PW exhibits strong spatial variability, supporting the use of the Monitoring Station as the site for studying PW seasonality. In contrast, WGIW properties fall along a narrow Θ–S_A line, and spatial variance along depth levels is small below 300 m, supporting the use of float data to characterise WGIW seasonality.

At depths $>$ 300 m, WGIW is isolated by bathymetry and is renewed when denser waters cross Egedesminde Dyb Sill (EDS). Our observations reveal that ~~West Greenland Irminger Water (WGIW) renewal occurs annuallyin~~ WGIW is renewed annually. Renewal occurs in the spring, with ~~one episodic~~ an additional episode of renewal also observed in late autumn ~~. In~~ 2022. During spring, the densest WGIW fills the Disko Bay basin, peaking in temperature, salinity, and vertical extent by late spring/early summer. ~~This provides observational evidence that WGIW renews in Disko Bay in spring, reflecting the seasonality of WGIW within West Greenland Current. An early renewal event observed in late autumn~~ The seasonal springtime renewal, previously

suggested by Gladish et al. (2015a), is confirmed by our observations. Its timing is consistent with regional isopycnal uplift and densification along the west Greenland shelf. The distinct autumn/winter renewal in November–December 2022 ~~, likely driven by upwelling-favourable winds,~~ coincided with unusually strong and persistent northerly winds over the EDS, which likely lifted denser waters over the topographic barrier, enabling the renewal. This suggests an additional mechanism and timing of ~~occasional~~ intermittent WGIW renewal in Disko Bay.

~~This new, observation-based~~ Overall, Disko Bay hydrography reflects the superposition of seasonal signals within WGC, spatially heterogeneous local freshwater inputs, local air- and ice-ocean interactions, and episodic wind-driven exchanges across EDS. The improved understanding of seasonality ~~provides a foundation for more accurate predictions of future variability. The significant impacts of both local and remote influences on the bay must be considered to make reliable predictions for the air-ice-ocean connectivity and its implications for the marine ecosystem of this region~~and spatial context provides a baseline for interpreting and predicting variability relevant to ice-ocean coupling and ecosystem dynamics within Disko Bay.

Data availability. The merged MODIS-AMSR2 sea-ice concentration data are available at: https://data.seaice.uni-bremen.de/modis_ amsr2. Greenland Ecosystem Monitoring (GEM) data are available at: https://data.g-e-m.dk/datasets. Additional observations collected for this study at the Monitoring Station in 2023 will be available through the GEM database. ERA5 data are available at the Copernicus Climate Change Service (C3S) Climate Data Store (CDS) (https://doi.org/10.24381/cds.adbb2d47, Copernicus Climate Change Service, Climate Data Store, 2023). Bathymetry data are available from the NASA National Snow and Ice Data Center Distributed Active Archive Center at: https://doi.org/10.5067/849. Oceans Melting Greenland Data for the profiling floats are available at: https://podaac.jpl.nasa.gov/dataset/OMG_L1_FLOAT_ Greenland Ocean Observations Apex-float data are available at: https://fleetmonitoring.euro-argo.eu/float/6990591.

Author contributions. LL: Writing – review and editing, Writing – original draft, Visualisation, Methodology, Investigation, Formal analysis, Conceptualisation. LH: Writing - review and editing, Writing – original draft, Methodology, Investigation, Conceptualisation, Supervision. ED: Writing - review and editing, Writing – original draft, Visualisation, Methodology, Investigation. PJH: Writing - review and editing, Resources, Data curation. JKW: Writing - review and editing, Resources, Data curation

Competing interests. The authors declare that they have no conflict of interest.

Acknowledgements. We thank Dana Margareta King for processing the sea-ice data, Iliana Vasiliki Ntinou for assisting with the fieldwork, and Torkel Gissel Nielsen for support with planning the fieldwork. We gratefully acknowledge the crew of RV *Porsild* and the staff at the Arctic Station (University of Copenhagen) in Qeqertarsuaq for their hard work and expertise in safely and effectively carrying out the fieldwork. We thank the NASA OMG Mission, as well as the GEM programme, for making observational data freely available. We acknowledge the collaborative efforts of scientists at the Greenland Institute of Natural Resources in collecting the NASA and NOAA

"Greenland Ocean Observations" (GOO) float data that contributed to this study. This work was carried out in part at the Jet Propulsion Laboratory, California Institute of Technology, under a contract with the National Aeronautics and Space Administration (80NM0018D0004). This work was supported financially by the Research Council of Norway through the project ClimateNarratives (no. 324520).

References

Andersen, O. G. N.: The annual cycle of temperature, salinity, currents and water masses in Disko Bugt and adjacent waters, West Greenland, Meddelelser om Grønland. Bioscience, 5, 1–33, https://doi.org/10.7146/mogbiosci.v5.142180, 1981a.

Andersen, O. G. N.: The annual cycle of phytoplankton primary production and hydrography in the Disko Bugt area, West Greenland, Meddelelser om Grønland. Bioscience, 6, 1–65., https://doi.org/10.7146/mogbiosci.v6.142187, 1981b.

Argo: Argo float data and metadata from Global Data Assembly Centre (Argo GDAC), https://doi.org/10.17882/42182, 2024.

Beaird, N., Straneo, F., and Jenkins, W.: Spreading of Greenland meltwaters in the ocean revealed by noble gases, Geophysical Research Letters, 42, 7705–7713, https://doi.org/10.1002/2015GL065003, 2015.

Beaird, N., Straneo, F., and Jenkins, W.: Characteristics of meltwater export from Jakobshavn Isbræ and Ilulissat Icefjord, Annals of Glaciology, 58, 107–117, https://doi.org/10.1017/aog.2017.19, 2017.

Beaird, N., Straneo, F., and Jenkins, W.: Export of Strongly Diluted Greenland Meltwater From a Major Glacial Fjord, Geophysical Research Letters, 45, 4163–4170, https://doi.org/10.1029/2018GL077000, 2018.

Carroll, D., Sutherland, D. A., Hudson, B., Moon, T., Catania, G. A., Shroyer, E. L., Nash, J. D., Bartholomaus, T. C., Felikson, D., Stearns, L. A., Noël, B. P. Y., and van den Broeke, M. R.: The impact of glacier geometry on meltwater plume structure and submarine melt in Greenland fjords, Geophysical Research Letters, 43, 9739–9748, https://doi.org/10.1002/2016GL070170, 2016.

Carroll, D., Sutherland, D. A., Shroyer, E. L., Nash, J. D., Catania, G. A., and Stearns, L. A.: Subglacial discharge-driven renewal of tidewater glacier fjords, Journal of Geophysical Research: Oceans, 122, 6611–6629, https://doi.org/10.1002/2017JC012962, 2017.

Carroll, D., Sutherland, D. A., Curry, B., Nash, J. D., Shroyer, E. L., Catania, G. A., Stearns, L. A., Grist, J. P., Lee, C. M., and de Steur, L.: Subannual and Seasonal Variability of Atlantic-Origin Waters in Two Adjacent West Greenland Fjords, Journal of Geophysical Research: Oceans, 123, 6670–6687, https://doi.org/10.1029/2018JC014278, 2018.

Cenedese, C. and Straneo, F.: Icebergs Melting, Annual Review of Fluid Mechanics, 55, 377–402, https://doi.org/10.1146/annurev-fluid-032522-100734, publisher: Annual Reviews, 2023.

Cowton, T., Slater, D., Sole, A., Goldberg, D., and Nienow, P.: Modeling the impact of glacial runoff on fjord circulation and submarine melt rate using a new subgrid-scale parameterization for glacial plumes, Journal of Geophysical Research: Oceans, 120, 796–812, https://doi.org/10.1002/2014JC010324, 2015.

Cowton, T. R., Slater, D. A., and Inall, M. E.: Subglacial-Discharge Plumes Drive Widespread Subsurface Warming in Northwest Greenland's Fjords, Geophysical Research Letters, 50, e2023GL103 801, https://doi.org/10.1029/2023GL103801, 2023.

Cuny, J., Rhines, P. B., and Ron Kwok: Davis Strait volume, freshwater and heat fluxes, Deep Sea Research Part I: Oceanographic Research Papers, 52, 519–542, https://doi.org/10.1016/j.dsr.2004.10.006, 2005.

Curry, B., Lee, C. M., and Petrie, B.: Volume, Freshwater, and Heat Fluxes through Davis Strait, 2004–05, https://doi.org/10.1175/2010JPO4536.1, section: Journal of Physical Oceanography, 2011.

Curry, B., Lee, C. M., Petrie, B., Moritz, R. E., and Kwok, R.: Multiyear Volume, Liquid Freshwater, and Sea Ice Transports through Davis Strait, 2004–10, https://doi.org/10.1175/JPO-D-13-0177.1, journal of Physical Oceanography, 2014.

Enderlin, E. M., Hamilton, G. S., Straneo, F., and Sutherland, D. A.: Iceberg meltwater fluxes dominate the freshwater budget in Greenland's iceberg-congested glacial fjords, Geophysical Research Letters, 43, 11,287–11,294, https://doi.org/10.1002/2016GL070718, 2016.

Foukal, N. P. and Pickart, R. S.: Moored Observations of the West Greenland Coastal Current along the Southwest Greenland Shelf, https://doi.org/10.1175/JPO-D-23-0104.1, section: Journal of Physical Oceanography, 2023.

Gade, H. G.: Melting of Ice in Sea Water: A Primitive Model with Application to the Antarctic Ice Shelf and Icebergs, https://journals.ametsoc.org/view/journals/phoc/9/1/1520-0485_1979_009_0189_moiisw_2_0_co_2.xml, journal of Physical Oceanography, 1979.

Gade, H. G. and Edwards, A.: Deep Water Renewal in Fjords, in: Fjord Oceanography, edited by Freeland, H. J., Farmer, D. M., and Levings, C. D., pp. 453–489, Springer US, Boston, MA, https://doi.org/10.1007/978-1-4613-3105-6_43, 1980.

Gladish, C. V., Holland, D. M., and Lee, C. M.: Oceanic Boundary Conditions for Jakobshavn Glacier. Part II: Provenance and Sources of Variability of Disko Bay and Ilulissat Icefjord Waters, 1990–2011, Journal of Physical Oceanography, 45, 33–63, https://doi.org/10.1175/JPO-D-14-0045.1, 2015a.

Gladish, C. V., Holland, D. M., Rosing-Asvid, A., Behrens, J. W., and Boje, J.: Oceanic Boundary Conditions for Jakobshavn Glacier. Part I: Variability and Renewal of Ilulissat Icefjord Waters, 2001–14, Journal of Physical Oceanography, 45, 3–32, https://doi.org/10.1175/JPO-D-14-0044.1, 2015b.

Gou, R., Pennelly, C., and Myers, P. G.: The Changing Behavior of the West Greenland Current System in a Very High-Resolution Model, Journal of Geophysical Research: Oceans, 127, e2022JC018 404, https://doi.org/10.1029/2022JC018404, _eprint: https://onlinelibrary.wiley.com/doi/pdf/10.1029/2022JC018404, 2022.

Greenland Ecosystem Monitoring: MarineBasis Disko - Water column - CTD measurements (Version 1.0) [Data set], https://doi.org/10.17897/WH30-HT61, 2025a.

Greenland Ecosystem Monitoring: MarineBasis Disko - Water column - Disko Bay Cruise 2018, CTD measurements (Version 1.0). [Data set], https://doi.org/10.17897/75KS-G922, 2025b.

Hager, A. O., Sutherland, D. A., and Slater, D. A.: Local forcing mechanisms challenge parameterizations of ocean thermal forcing for Greenland tidewater glaciers, The Cryosphere, 18, 911–932, https://doi.org/10.5194/tc-18-911-2024, publisher: Copernicus GmbH, 2024.

Hansen, M. O., Nielsen, T. G., Stedmon, C. A., and Munk, P.: Oceanographic regime shift during 1997 in Disko Bay, Western Greenland, Limnology and Oceanography, 57, 634–644, https://www.jstor.org/stable/26954126, 2012.

Hersbach, H., Bell, B., Berrisford, P., Biavati, G., Horányi, A., Muñoz Sabater, J., Nicolas, J., Peubey, C., Radu, R., Rozum, I., Schepers, D., Simmons, A., Soci, C., Dee, D., and Thépaut, J-N.: ERA5 hourly data on single levels from 1940 to present, DOI:10.24381/cds.adbb2d47, 2023.

Holland, D. M., Thomas, R. H., de Young, B., Ribergaard, M. H., and Lyberth, B.: Acceleration of Jakobshavn Isbræ triggered by warm subsurface ocean waters, Nature Geoscience, 1, 659–664, https://doi.org/10.1038/ngeo316, 2008.

Hopwood, M. J., Carroll, D., Gu, Y., Huang, X., Krause, J., Cozzi, S., Cantoni, C., Gastelu Barcena, M. F., Carroll, S., and Körtzinger, A.: A Close Look at Dissolved Silica Dynamics in Disko Bay, West Greenland, Global Biogeochemical Cycles, 39, e2023GB008 080, https://doi.org/10.1029/2023GB008080, 2025.

Huang, J., Pickart, R. S., Bahr, F., McRaven, L. T., Tremblay, J.-, Michel, C., Jeansson, E., Kopec, B., Welker, J. M., and Ólafsdóttir, S. R.: Water mass evolution and general circulation of Baffin Bay: Observations from two shipboard surveys in 2021, Progress in Oceanography, p. 103322, https://doi.org/10.1016/j.pocean.2024.103322, 2024.

Jackson, R. H., Shroyer, E. L., Nash, J. D., Sutherland, D. A., Carroll, D., Fried, M. J., Catania, G. A., Bartholomaus, T. C., and Stearns, L. A.: Near-glacier surveying of a subglacial discharge plume: Implications for plume parameterizations, Geophysical Research Letters, 44, 6886–6894, https://doi.org/10.1002/2017GL073602, 2017.

Jenkins, A.: Convection-Driven Melting near the Grounding Lines of Ice Shelves and Tidewater Glaciers, https://doi.org/10.1175/JPO-D-11-03.1, 2011.

Joughin, I., Abdalati, W., and Fahnestock, M.: Large fluctuations in speed on Greenland's Jakobshavn Isbræ glacier, Nature, 432, 608–610, https://doi.org/10.1038/nature03130, 2004.

Joughin, I., Smith, B. E., and Howat, I.: Greenland Ice Mapping Project: ice flow velocity variation at sub-monthly to decadal timescales, The Cryosphere, 12, 2211–2227, https://doi.org/10.5194/tc-12-2211-2018, 2018.

Joughin, I., Shean, D. E., Smith, B. E., and Floricioiu, D.: A decade of variability on Jakobshavn Isbræ: ocean temperatures pace speed through influence on mélange rigidity, The Cryosphere, 14, 211–227, https://doi.org/10.5194/tc-14-211-2020, 2020.

Kajanto, K., Straneo, F., and Nisancioglu, K.: Impact of icebergs on the seasonal submarine melt of Sermeq Kujalleq, The Cryosphere, 17, 371–390, https://doi.org/10.5194/tc-17-371-2023, 2023.

Khazendar, A., Fenty, I. G., Carroll, D., Gardner, A., Lee, C. M., Fukumori, I., Wang, O., Zhang, H., Seroussi, H., Moller, D., Noël, B. P. Y., van den Broeke, M. R., Dinardo, S., and Willis, J.: Interruption of two decades of Jakobshavn Isbrae acceleration and thinning as regional ocean cools, Nature Geoscience, 12, 277–283, https://doi.org/10.1038/s41561-019-0329-3, 2019.

Killick, R., Fearnhead, P., and Eckley, I. A.: Optimal Detection of Changepoints With a Linear Computational Cost, Journal of the American Statistical Association, 107, 1590–1598, https://doi.org/10.1080/01621459.2012.737745, 2012.

Lavielle, M.: Using penalized contrasts for the change-point problem, Signal Processing, 85, 1501–1510, https://doi.org/10.1016/j.sigpro.2005.01.012, 2005.

Lindeman, M. R., Straneo, F., Adams, H. M., Nelson, M. J. S., and Schartup, A. T.: Low mercury concentrations in a Greenland glacial fjord attributed to oceanic sources, Communications Earth & Environment, 5, 1–10, https://doi.org/10.1038/s43247-024-01474-9, 2024.

Ludwig, V., Spreen, G., and Pedersen, L. T.: Evaluation of a New Merged Sea-Ice Concentration Dataset at 1 km Resolution from Thermal Infrared and Passive Microwave Satellite Data in the Arctic, Remote Sensing, 12, 3183, https://doi.org/10.3390/rs12193183, 2020.

Lüpkes, C. and Birnbaum, G.: Surface Drag in the Arctic Marginal Sea-ice Zone: A Comparison of Different Parameterisation Concepts, Boundary-Layer Meteorology, 117, 179–211, https://doi.org/10.1007/s10546-005-1445-8, 2005.

Mankoff, K. D., Straneo, F., Cenedese, C., Das, S. B., Richards, C. G., and Singh, H.: Structure and dynamics of a subglacial discharge plume in a Greenlandic fjord, Journal of Geophysical Research: Oceans, 121, 8670–8688, https://doi.org/10.1002/2016JC011764, 2016.

Mankoff, K. D., Solgaard, A., Colgan, W., Ahlstrøm, A. P., Khan, S. A., and Fausto, R. S.: Greenland Ice Sheet solid ice discharge from 1986 through March 2020, Earth System Science Data, 12, 1367–1383, https://doi.org/10.5194/essd-12-1367-2020, 2020.

McDougall, T. J. and Barker, P. M.: Getting started with TEOS-10 and the Gibbs Seawater (GSW) Oceanographic Toolbox, 28pp, www.TEOS-10.org, 2011.

Mernild, S. H., Holland, D. M., Holland, D., Rosing-Asvid, A., Yde, J. C., Liston, G. E., and Steffen, K.: Freshwater Flux and Spatiotemporal Simulated Runoff Variability into Ilulissat Icefjord, West Greenland, Linked to Salinity and Temperature Observations near Tidewater Glacier Margins Obtained Using Instrumented Ringed Seals, https://doi.org/10.1175/JPO-D-14-0217.1, 2015.

Moon, T., Sutherland, D. A., Carroll, D., Felikson, D., Kehrl, L., and Straneo, F.: Subsurface iceberg melt key to Greenland fjord freshwater budget, Nature Geoscience, 11, 49–54, https://doi.org/10.1038/s41561-017-0018-z, 2018.

Morlighem, M., Williams, C., Rignot, E., An, L., Arndt, J., Bamber, J., Catania, G., Chauché, N., Dowdeswell, J., Dorschel, B., Fenty, I., Hogan, K., Howat, I., Hubbard, A., Jakobsson, M., Jordan, T., Kjeldsen, K., Millan, R., Mayer, L., Mouginot, J., Noël, B., O'Cofaigh, C., Palmer, S., Rysgaard, S., Seroussi, H., Siegert, M., Slabon, P., Straneo, F., van den Broeke, M., Weinrebe, W., Wood, M., and Zinglersen, K.: IceBridge BedMachine Greenland. (IDBMG4, Version 5). [Data Set]., https://doi.org/10.5067/GMEVBWFLWA7X, 2022.

Mortensen, J., Lennert, K., Bendtsen, J., and Rysgaard, S.: Heat sources for glacial melt in a sub-Arctic fjord (Godthåbsfjord) in contact with the Greenland Ice Sheet, Journal of Geophysical Research: Oceans, 116, https://doi.org/10.1029/2010JC006528, 2011.

Mortensen, J., Bendtsen, J., Lennert, K., and Rysgaard, S.: Seasonal variability of the circulation system in a west Greenland tidewater outlet glacier fjord, Godthåbsfjord (64°N), Journal of Geophysical Research: Earth Surface, 119, 2591–2603, https://doi.org/10.1002/2014JF003267, 2014.

Mortensen, J., Rysgaard, S., Bendtsen, J., Lennert, K., Kanzow, T., Lund, H., and Meire, L.: Subglacial Discharge and Its Down-Fjord Transformation in West Greenland Fjords With an Ice Mélange, Journal of Geophysical Research: Oceans, 125, e2020JC016 301, https://doi.org/10.1029/2020JC016301, 2020.

Motyka, R. J., Truffer, M., Fahnestock, M., Mortensen, J., Rysgaard, S., and Howat, I.: Submarine melting of the 1985 Jakobshavn Isbræ floating tongue and the triggering of the current retreat, Journal of Geophysical Research: Earth Surface, 116, https://doi.org/10.1029/2009JF001632, 2011.

Muench, R. D.: Oceanographic observations in Baffin Bay during July-September 1968, Washington, D.C. : Coast Guard, Oceanographic Unit, 1971.

Muilwijk, M., Straneo, F., Slater, D. A., Smedsrud, L. H., Holte, J., Wood, M., Andresen, C. S., and Harden, B.: Export of Ice Sheet Meltwater from Upernavik Fjord, West Greenland, Journal of Physical Oceanography, 52, 363–382, https://doi.org/10.1175/JPO-D-21-0084.1, 2022.

Myers, P. G. and Ribergaard, M. H.: Warming of the Polar Water Layer in Disko Bay and Potential Impact on Jakobshavn Isbrae, Journal of Physical Oceanography, 43, 2629–2640, https://doi.org/10.1175/JPO-D-12-051.1, 2013.

Nielsen TG and Hansen B: Plankton community structure and carbon cycling on the western coast of Greenland during and after the sedimentation of a diatom bloom, Marine Ecology Progress Series, 125, 239–257, https://www.int-res.com/abstracts/meps/v125/p239-257/, 1995.

Oceans Melting Greenland: OMG Ocean Water Properties Data from Alamo Floats Version 1. Ver. 1., https://doi.org/10.5067/OMGEV-ALMO1, 2022.

Oliver, H., Slater, D., Carroll, D., Wood, M., Morlighem, M., and Hopwood, M. J.: Greenland Subglacial Discharge as a Driver of Hotspots of Increasing Coastal Chlorophyll Since the Early 2000s, Geophysical Research Letters, 50, e2022GL102 689, https://doi.org/10.1029/2022GL102689, 2023.

Pacini, A. and Pickart, R. S.: Wind-Forced Upwelling Along the West Greenland Shelfbreak: Implications for Labrador Sea Water Formation, Journal of Geophysical Research: Oceans, 128, e2022JC018 952, https://doi.org/10.1029/2022JC018952, 2023.

Pacini, A., Pickart, R. S., Bahr, F., Torres, D. J., Ramsey, A. L., Holte, J., Karstensen, J., Oltmanns, M., Straneo, F., Bras, I. A. L., Moore, G. W. K., and Jong, M. F. d.: Mean Conditions and Seasonality of the West Greenland Boundary Current System near Cape Farewell, https://doi.org/10.1175/JPO-D-20-0086.1, 2020.

Petersen, G.: The hydrography, primary production, bathymetry and "Tagsaq" of Disko Bugt, West Greenland, 159, 1–45, 1964.

Pickart, R. S., Torres, D. J., and Clarke, R. A.: Hydrography of the Labrador Sea during Active Convection, 2002.

Picton, H. J., Nienow, P. W., Slater, D. A., and Chudley, T. R.: A Reassessment of the Role of Atmospheric and Oceanic Forcing on Ice Dynamics at Jakobshavn Isbræ (Sermeq Kujalleq), Ilulissat Icefjord, Journal of Geophysical Research: Earth Surface, 130, e2024JF008 104, https://doi.org/10.1029/2024JF008104, 2025.

Ribergaard, M. H., Pedersen, A. S., Ådlandsvik, B., and Kliem, N.: Modelling the ocean circulation on the West Greenland shelf with special emphasis on northern shrimp recruitment, Continental Shelf Research, 24, 1505–1519, https://doi.org/10.1016/j.csr.2004.05.011, 2004.

Rysgaard, S., Boone, W., Carlson, D., Sejr, M. K., Bendtsen, J., Juul-Pedersen, T., Lund, H., Meire, L., and Mortensen, J.: An Updated View on Water Masses on the pan-West Greenland Continental Shelf and Their Link to Proglacial Fjords, Journal of Geophysical Research: Oceans, 125, e2019JC015 564, https://doi.org/10.1029/2019JC015564, 2020.

Sanchez, R., Straneo, F., Hughes, K., Barbour, P., and Shroyer, E.: Relative Roles of Plume and Coastal Forcing on Exchange Flow Variability of a Glacial Fjord, Journal of Geophysical Research: Oceans, 129, e2023JC020 492, https://doi.org/10.1029/2023JC020492, 2024.

Scheick, J., Enderlin, E. M., and Hamilton, G.: Semi-automated open water iceberg detection from Landsat applied to Disko Bay, West Greenland, Journal of Glaciology, 65, 468–480, https://doi.org/10.1017/jog.2019.23, 2019.

Semper, S., Våge, K., Fer, I., Latuta, L., and Skjelsvik, S.: Formation and circulation of dense water from a two-year moored record in the northwestern Iceland Sea, Manuscript in review in Journal of Geophysical Research: Oceans, 2024.

Slater, D. A., Carroll, D., Oliver, H., Hopwood, M. J., Straneo, F., Wood, M., Willis, J. K., and Morlighem, M.: Characteristic Depths, Fluxes, and Timescales for Greenland's Tidewater Glacier Fjords From Subglacial Discharge-Driven Upwelling During Summer, Geophysical Research Letters, 49, e2021GL097 081, https://doi.org/10.1029/2021GL097081, 2022.

Sloth, P. and Buch, E.: On the hydrography and watermass exchange of Disko Bay, https://ices.dk/sites/pub/CM%20Doccuments/1984/C/1984_C26.pdf, 1984.

Snow, T., Zhang, W., Schreiber, E., Siegfried, M., Abdalati, W., and Scambos, T.: Alongshore Winds Force Warm Atlantic Water Toward Helheim Glacier in Southeast Greenland, Journal of Geophysical Research: Oceans, 128, e2023JC019 953, https://doi.org/10.1029/2023JC019953, 2023.

Stevens, L. A., Straneo, F., Das, S. B., Plueddemann, A. J., Kukulya, A. L., and Morlighem, M.: Linking glacially modified waters to catchment-scale subglacial discharge using autonomous underwater vehicle observations, The Cryosphere, 10, 417–432, https://doi.org/10.5194/tc-10-417-2016, 2016.

Straneo, F. and Cenedese, C.: The Dynamics of Greenland's Glacial Fjords and Their Role in Climate, Annual Review of Marine Science, 7, 89–112, https://doi.org/10.1146/annurev-marine-010213-135133, 2015.

Straneo, F., Curry, R. G., Sutherland, D. A., Hamilton, G. S., Cenedese, C., Våge, K., and Stearns, L. A.: Impact of fjord dynamics and glacial runoff on the circulation near Helheim Glacier, Nature Geoscience, 4, 322–327, https://doi.org/10.1038/ngeo1109, 2011.

Straneo, F., Sutherland, D. A., Holland, D., Gladish, C., Hamilton, G. S., Johnson, H. L., Rignot, E., Xu, Y., and Koppes, M.: Characteristics of ocean waters reaching Greenland's glaciers, Annals of Glaciology, 53, 202–210, https://doi.org/10.3189/2012AoG60A059, 2012.

Söderkvist, J., Nielsen, T. G., and Jespersen, M.: Physical and biological oceanography in West Greenland waters with emphasis on shrimp and fish larvae distribution, Tech. Rep. NERI Technical Report No. 581, National Environmental Research Institute, Denmark, 2006.

Wong, A., Keeley, R., and Carval, T.: Argo Quality Control Manual for CTD and Trajectory Data, https://doi.org/10.13155/33951, 2024.

Wood, M., Rignot, E., Fenty, I., An, L., Bjørk, A., Van Den Broeke, M., Cai, C., Kane, E., Menemenlis, D., Millan, R., Morlighem, M., Mouginot, J., Noël, B., Scheuchl, B., Velicogna, I., Willis, J. K., and Zhang, H.: Ocean forcing drives glacier retreat in Greenland, Science Advances, 7, https://doi.org/10.1126/sciadv.aba7282, 2021.

Wood, M., Carroll, D., Fenty, I., Bertin, C., Darby, B., Dutkiewicz, S., Hopwood, M., Khazendar, A., Meire, L., Oliver, H., Parker, T., and Willis, J.: Increased melt from Greenland's most active glacier fuels enhanced coastal productivity, Communications Earth & Environment, 6, 626, https://doi.org/10.1038/s43247-025-02599-1, 2025.

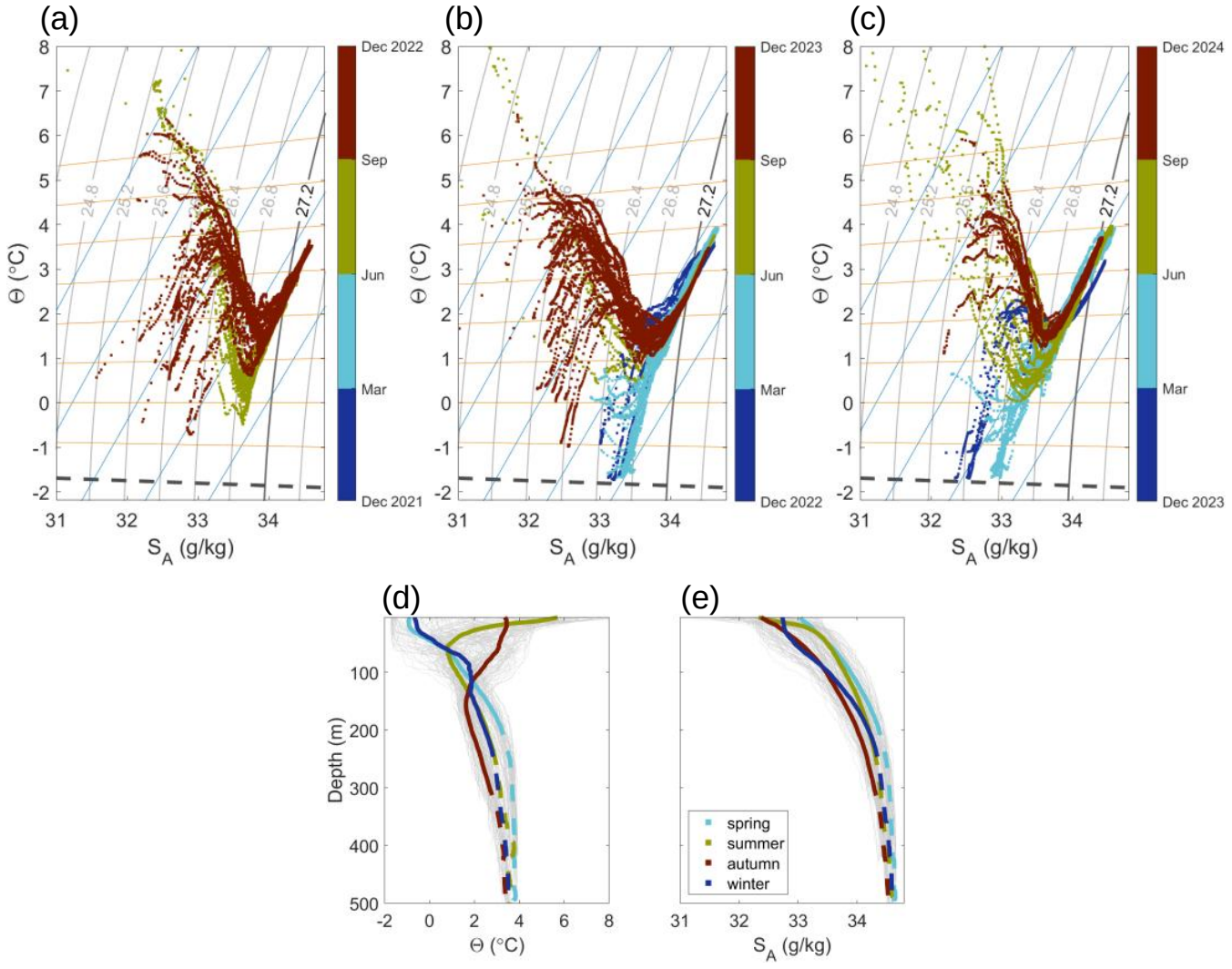

Figure 3. (aa–c) ~~Temperature~~ Temperature–Salinity (Θ) ~~- Salinity (~~–S_A) ~~diagram for all~~ diagrams from Monitoring Station and float observations ~~between~~ for annual cycles spanning June 2022 ~~and October~~ - November 2024 (~~dots~~ circle markers coloured by ~~depth~~season). Grey contours ~~show~~ are isopycnals at ~~0.2~~0.4 kg m^{-3} intervals~~refereneed to surface pressure. The~~ ; the thick grey line at 27.2 kg m^{-3} ~~isopycnal is marked (thick grey line) as it~~ delineates West Greenland Irminger Water (WGIW) ~~and~~ from Polar Water (PW). ~~Dashed~~ Orange and blue lines ~~show~~ indicate mixing lines ~~between the mean WGIW properties and Subglacial Discharge~~ with subglacial discharge/runoff (~~SGD~~Θ = 0°C, ~~Red~~S_A = 0 g kg^{-1}) and ~~Submarine Meltwater~~ submarine meltwater (~~SMW~~Θ = -90°C, ~~Blue~~S_A = 0 g kg^{-1}), respectively. ~~Yellow shading between these two mixing lines marks the typical properties of glacially modified waters (GMW).~~ The ~~dotted green~~ dashed grey line marks the surface freezing point. (~~bd~~–e) ~~Temperature~~ Vertical temperature and salinity profiles from ~~Disko Bay~~ all observations in (a–c) (thin grey lines), overlaid ~~by a~~ with mean ~~profile~~ seasonal profiles (thick ~~black~~ coloured lines~~). Red and blue shadings mark WGIW and PW~~, ~~respectively,~~ with ~~the boundary defined by the density of the mean profile~~solid segments corresponding to PW and dashed segments to WGIW).

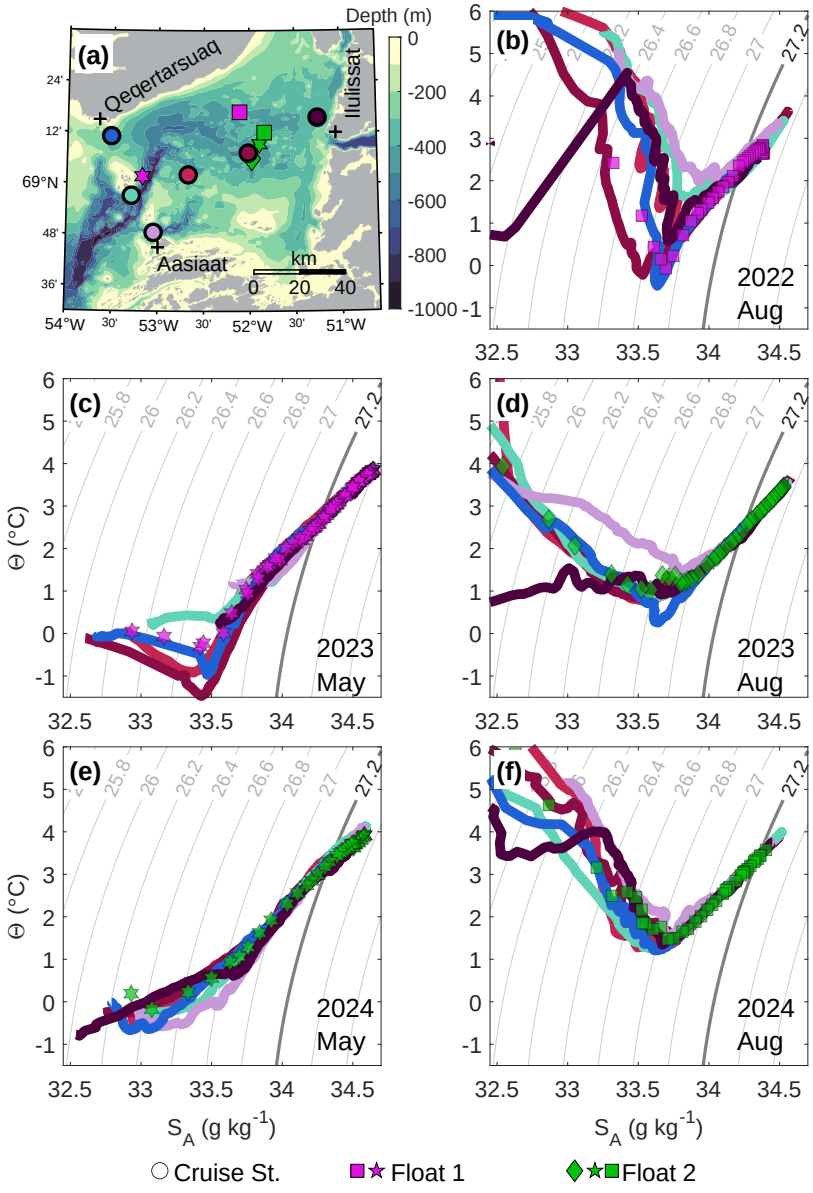

Figure 4. ~~Hydrography in~~ Spatial hydrographic variability across Disko Bay from ~~June 2022 to October 2024. Temperature for the monitoring station~~ GEM spatial surveys (~~a~~2022–2024) and ~~profiling floats~~ float observations. (~~b~~a) ~~. Salinity for the monitoring~~ Map of station locations (~~c~~circle markers). Float 1 profiles are shown as magenta markers (square, pentagram) and ~~profiling floats~~ Float 2 as green markers (~~d~~diamond, pentagram, square). ~~Buoyancy frequency for the monitoring station~~ (~~e~~b–f) ~~and profiling floats~~ Temperature–Salinity (~~f~~~~Θ~~–S_A) diagrams for each cruise. ~~Temperature, Salinity, and Buoyancy Frequency are overlaid by labelled isopycnals~~ Left column: May (~~blue thick line σ_0= 27.2 kg m^{-3} showing the upper WGIW boundary~~2023, 2024)~~and mixed-layer depth~~ . Right column: August (~~white lines~~2022, 2023, 2024). ~~Vertical ticks on the upper x-axis~~ Coloured lines and float markers correspond to stations and colours shown in (a)~~ (f)~~ . Grey contours show isopycnals, with the ~~time of profile acquisitions~~ thick grey contour delineating West Greenland Irminger Water (~~blue - monitoring station, pink - Float 1, green - Float 2~~WGIW) ~~, while dashed vertical lines through all panels mark the start of each calendar year~~and Polar Water (PW).

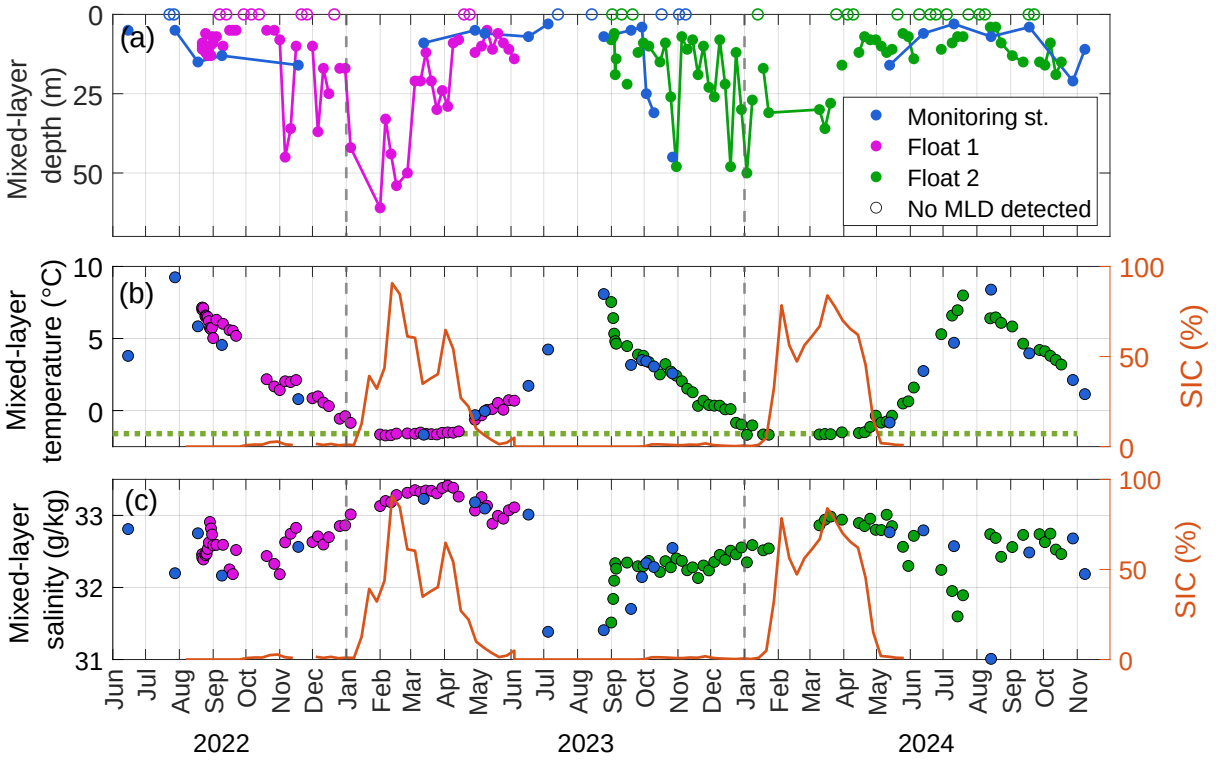

Figure 5. Time series of ~~Disko Bay~~ mixed-layer properties ~~between 2022–2024, with~~ in Disko Bay from 2022 to 2024. (a) Mixed-layer depth (MLD), (b) mixed-layer temperature, and (c) mixed-layer salinity. Sea-ice concentration ~~inside~~ (SIC) within Disko Bay is shown in orange (right axis in ~~b~~(b–c)~~and c~~). ~~Observed profiles~~ Data are from the ~~monitoring station~~ Monitoring Station (blue)~~and two floats (pink –~~, Float 1 (magenta), ~~green –~~ and Float 2 (green). Empty circle markers in (a) indicate times when the mixed layer was not detectable.

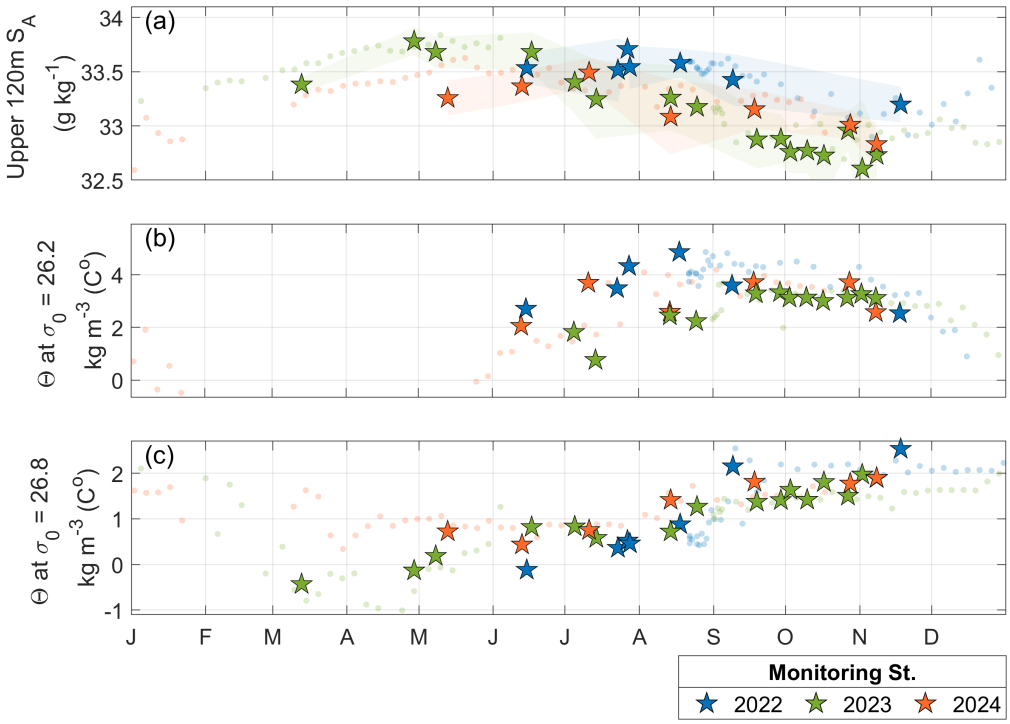

Figure 6. ~~Spatial analysis~~ Seasonal cycle of ~~two survey cruises in Disko Bay in 2018.~~ (a) ~~The map shows survey stations from~~ mean salinity in the ~~May~~ upper 120 m (~~grey dots~~one standard deviation shaded in the background)~~and August (black dots) cruises~~, ~~divided into three regions: eastern~~ (~~pink box~~b) along-isopycnal temperature at $\sigma_0 = 26.2$ kg m^{-3}, ~~northern (blue box),~~ and ~~central~~ (~~black box~~c) along-isopycnal temperature at $\sigma_0 = 26.8$ kg m^{-3}. ~~The results are displayed~~ Monitoring Station observations for ~~May (b–e) and August (f–i)~~2022, ~~depicting temperature (b~~2023, ~~f)~~and 2024 are shown with blue, ~~salinity (e~~green, ~~g),~~ and ~~density profiles (d~~orange star markers, ~~h), with each profile colour-coded by region~~respectively. ~~The green dashed line indicates the depth of the Ilulissat Icefjord Sill (~240 m). Along-isopycnal temperature anomalies (ΔΘ) relative to the central region in May (e)~~ Faint background markers show Float 1 and ~~August (i) as a function of density~~2 observations, ~~with thin lines showing ΔΘ~~ included here for ~~each profile and a thick line showing the regional mean~~reference.~~Positive ΔΘ anomalies are identified from the mean (e, i) and the depth range of these densities is shaded in (d,h), colour-coded by region.~~

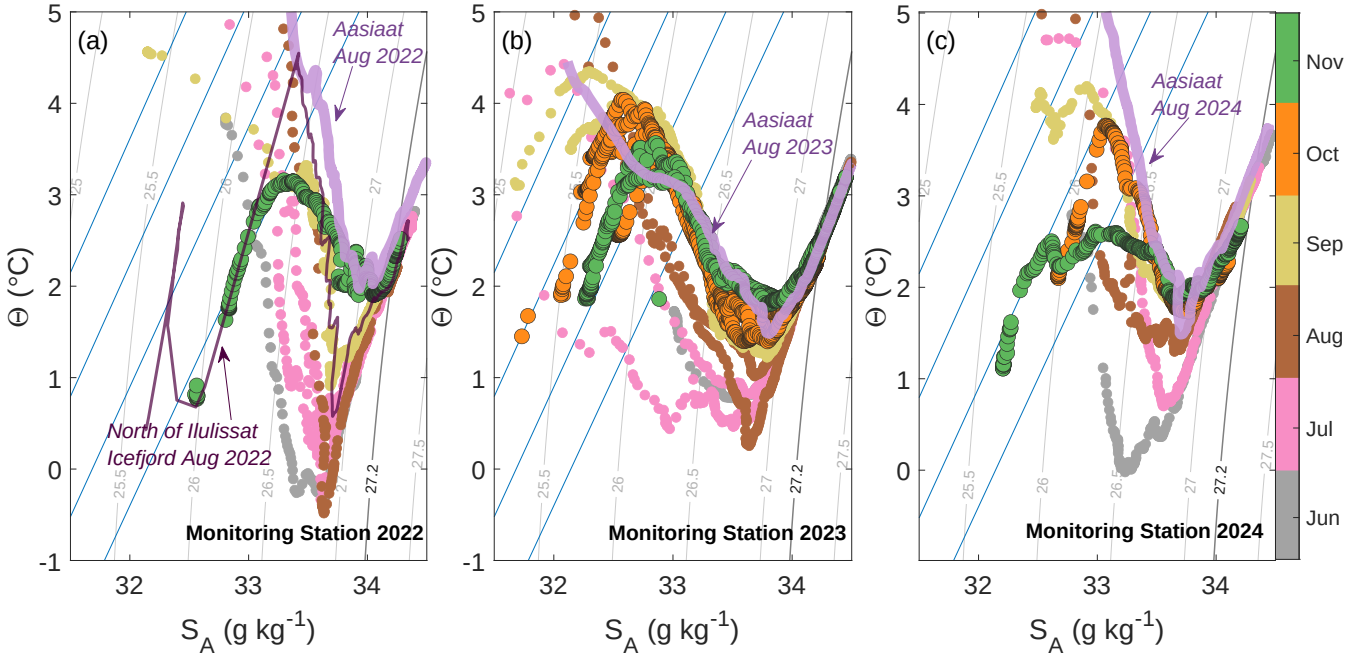

Figure 7. ~~Seasonal cycle of along-isopycnal temperature at~~ Temperature - Salinity (a~~Θ~~-S_A) ~~σ_0 = 26.8 kg m^{-3} and~~ diagrams for the Monitoring Station for (~~b~~a) ~~σ_0 = 27 kg m^{-3} isopycnals. The seasonal cycles of~~ 2022, (b) 2023, and (c) 2024, covering June–November. Circle markers are observations coloured by month; October-November are shown with ~~blue~~a black outline. The thick lilac line in panels (a–c) shows Θ-S_A properties at the station near Aasiaat during August of the same year (previously shown in Fig.4b, ~~greend~~, ~~and orange markers~~f); the thin purple line in (a) is the same, ~~respectively. Star markers are~~ but for the ~~monitoring~~ station ~~observations~~north of Ilulissat Icefjord. Isopycnals are shown in grey, ~~and circles for~~ with the ~~Float 1~~ thick contour delineating West Greenland Irminger Water (WGIW) and ~~2.~~Polar Water (PW). Submarine meltwater (Θ = -90°C, S_A = 0 g kg^{-1}) mixing lines are shown in blue

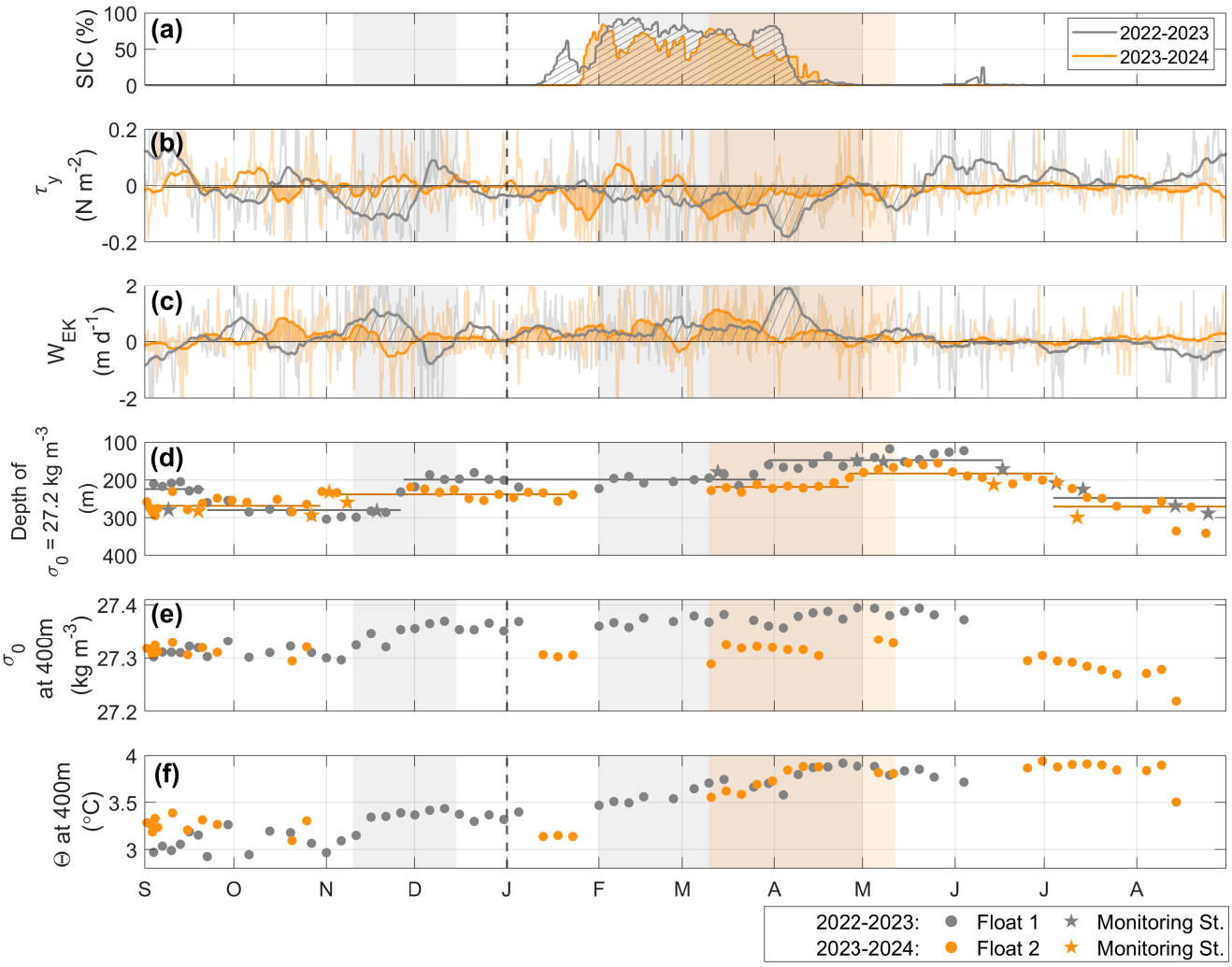

Figure 8. Seasonality of atmospheric forcing and WGIW properties in Disko Bay ~~based on~~ over two annual cycles ~~of observations~~ (2022–2023 in grey~~colours for 2022-2023~~, 2023–2024 in orange~~colours~~ , circle markers for ~~2023-2024~~the Floats, star markers for the Monitoring Station). Mean sea-ice cover (a), along-shore wind stress (τ_y) (b), and vertical velocity ~~W_E~~ W_E (Ekman pumping) over the EDS area (Fig. 1a) (c). In panels (~~b-c~~b–c), hourly data ~~in the background is~~ are overlaid ~~by~~ with a 10-day running mean ~~in~~ (thick lines~~. Shaded or~~); shaded and hatched areas highlight the negative and positive ranges in (b) and (c), respectively. Depth of the σ_0= 27.2 kg m^{-3} ~~-~~ upper WGIW boundary (d)~~for all observations~~, with horizontal lines indicating the mean depth before abrupt changes, identified using MATLAB findchangepts() function (Lavielle, 2005; Killick et al., 2012). Density (e) and temperature (f) at ~~400m~~ 400 m depth ~~. Background shading in (d-e) mark periods with renewal signatures, with grey for 2022-2023 renewals~~ from Float 1 and ~~orange for 2023-2024 renewals~~Float 2. Basin renewal periods are shaded in all panels. The dashed vertical line in all ~~plots~~ panels marks a new year.

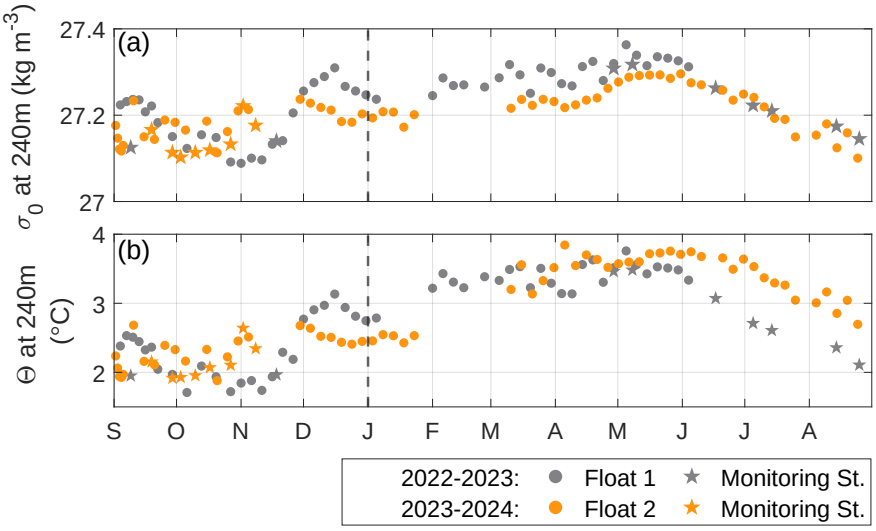

Figure 9. Seasonal cycle of ~~density~~ (a) density and ~~temperature~~ (b) temperature at ~~240m~~ 240 m depth, corresponding to the Ilulissat Icefjord Sill depth. Grey markers are observations from ~~2022-2023~~ 2022–2023, and orange from ~~2023-2024~~2023–2024. Star markers are for the ~~monitoring station~~ Monitoring Station observations, and circles for the ~~Float~~ Floats 1 and 2.

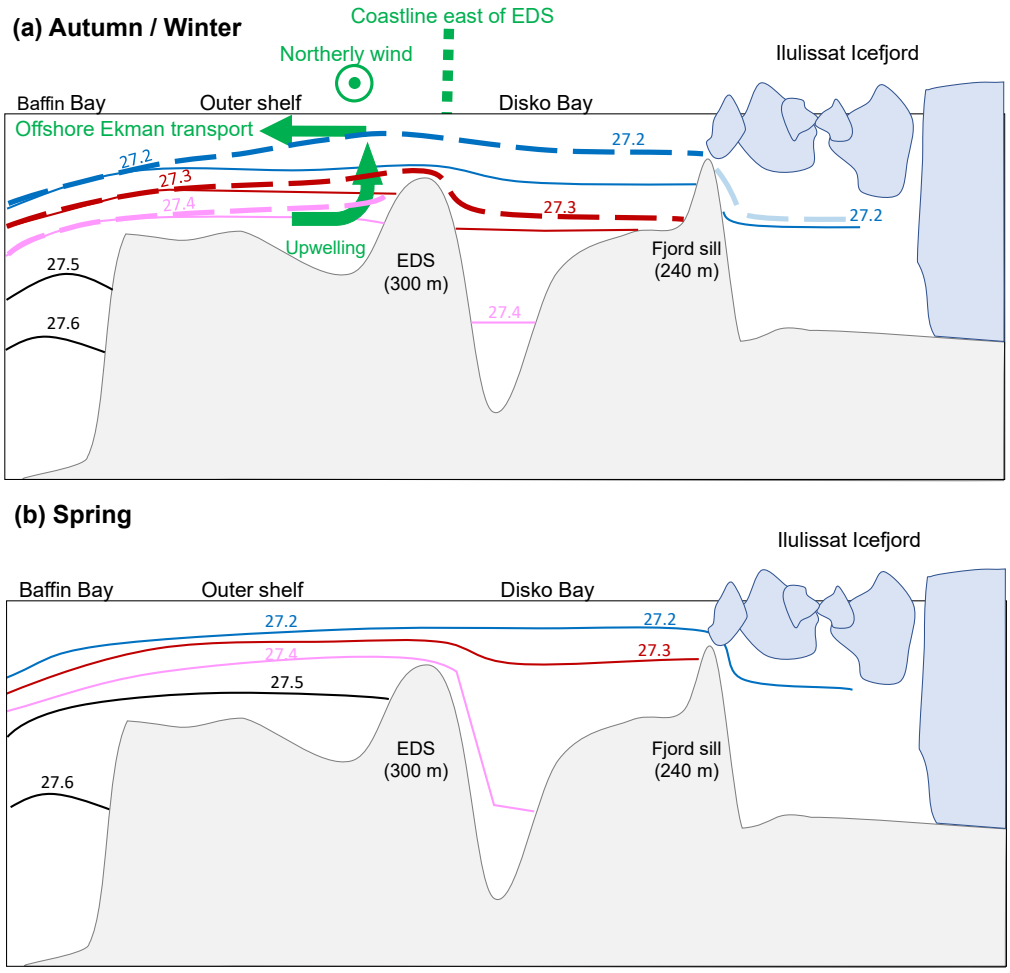

Figure 10. Schematic of West Greenland Irminger Water (WGIW) exchange between the west Greenland Shelf, Disko Bay, and Ilulissat Icefjord, adapted from Gladish et al. (2015a). Solid isopycnals and bathymetry in (a–b) are reproduced from the original schematic. Panel (a) has been updated to illustrate a potential autumn/winter wind-driven renewal mechanism: Northerly along-shore winds (negative wind stress, ⊙) drive offshore Ekman transport and upwelling (green arrows), lifting dense isopycnals over the Egedesminde Dyb Sill (EDS) and allowing renewal of Disko Bay (dashed lines), and possibly Ilulissat Icefjord (fainter dashed line). The coastline east of EDS is indicated as it likely enhances wind-driven upwelling. Panel (b) shows spring renewal process, when seasonal densification of WGIW on the west Greenland Shelf raises isopycnals above sill depth, enabling Disko Bay and Ilulissat Icefjord renewal.